EUROPEAN LABORATORY FOR PARTICLE PHYSICS

CERN-PPE/97-093
18-July-1997

Measurement of $f(c \to D^{*+}X)$, $f(b \to D^{*+}X)$ and $\Gamma_{c\bar{c}}/\Gamma_{had}$ using $D^{*\pm}$ Mesons

THE OPAL COLLABORATION

Abstract

The production rates of $D^{*\pm}$ mesons in charm and bottom events at centre-of-mass energies of about 91 GeV and the partial width of primary $c\bar{c}$ pairs in hadronic Z^0 decays have been measured at LEP using almost 4.4 million hadronic Z^0 decays collected with the OPAL detector between 1990 and 1995. Using a combination of several charm quark tagging methods based on fully and partially reconstructed $D^{*\pm}$ mesons, and a bottom tag based on identified muons and electrons, the hadronisation fractions of charm and bottom quarks into $D^{*\pm}$ mesons have been found to be

$$f\,(b \to D^{*+}X) = 0.173 \pm 0.016 \pm 0.012 \quad \text{and} \quad f\,(c \to D^{*+}X) = 0.222 \pm 0.014 \pm 0.014\ .$$

The fraction of $c\bar{c}$ events in hadronic Z^0 decays, $\Gamma_{c\bar{c}}/\Gamma_{had} = \Gamma(Z^0 \to c\bar{c})/\Gamma(Z^0 \to \text{hadrons})$, is determined to be

$$\Gamma_{c\bar{c}}/\Gamma_{had} = 0.180 \pm 0.011 \pm 0.012 \pm 0.006\ .$$

In all cases the first error is statistical, and the second one systematic. The last error quoted for $\Gamma_{c\bar{c}}/\Gamma_{had}$ is due to external branching ratios.

Submitted to Zeitschrift für Physik C

THE OPAL COLLABORATION

K. Ackerstaff[8], G. Alexander[23], J. Allison[16], N. Altekamp[5], K.J. Anderson[9], S. Anderson[12], S. Arcelli[2], S. Asai[24], D. Axen[29], G. Azuelos[18,a], A.H. Ball[17], E. Barberio[8], T. Barillari[2], R.J. Barlow[16], R. Bartoldus[3], J.R. Batley[5], S. Baumann[3], J. Bechtluft[14], C. Beeston[16], T. Behnke[8], A.N. Bell[1], K.W. Bell[20], G. Bella[23], S. Bentvelsen[8], S. Bethke[14], O. Biebel[14], A. Biguzzi[5], S.D. Bird[16], V. Blobel[27], I.J. Bloodworth[1], J.E. Bloomer[1], M. Bobinski[10], P. Bock[11], D. Bonacorsi[2], M. Boutemeur[34], B.T. Bouwens[12], S. Braibant[12], L. Brigliadori[2], R.M. Brown[20], H.J. Burckhart[8], C. Burgard[8], R. Bürgin[10], P. Capiluppi[2], R.K. Carnegie[6], A.A. Carter[13], J.R. Carter[5], C.Y. Chang[17], D.G. Charlton[1,b], D. Chrisman[4], P.E.L. Clarke[15], I. Cohen[23], J.E. Conboy[15], O.C. Cooke[8], M. Cuffiani[2], S. Dado[22], C. Dallapiccola[17], G.M. Dallavalle[2], R. Davis[30], S. De Jong[12], L.A. del Pozo[4], K. Desch[3], B. Dienes[33,d], M.S. Dixit[7], E. do Couto e Silva[12], M. Doucet[18], E. Duchovni[26], G. Duckeck[34], I.P. Duerdoth[16], D. Eatough[16], J.E.G. Edwards[16], P.G. Estabrooks[6], H.G. Evans[9], M. Evans[13], F. Fabbri[2], M. Fanti[2], A.A. Faust[30], F. Fiedler[27], M. Fierro[2], H.M. Fischer[3], I. Fleck[8], R. Folman[26], D.G. Fong[17], M. Foucher[17], A. Fürtjes[8], D.I. Futyan[16], P. Gagnon[7], J.W. Gary[4], J. Gascon[18], S.M. Gascon-Shotkin[17], N.I. Geddes[20], C. Geich-Gimbel[3], T. Geralis[20], G. Giacomelli[2], P. Giacomelli[4], R. Giacomelli[2], V. Gibson[5], W.R. Gibson[13], D.M. Gingrich[30,a], D. Glenzinski[9], J. Goldberg[22], M.J. Goodrick[5], W. Gorn[4], C. Grandi[2], E. Gross[26], J. Grunhaus[23], M. Gruwé[8], C. Hajdu[32], G.G. Hanson[12], M. Hansroul[8], M. Hapke[13], C.K. Hargrove[7], P.A. Hart[9], C. Hartmann[3], M. Hauschild[8], C.M. Hawkes[5], R. Hawkings[27], R.J. Hemingway[6], M. Herndon[17], G. Herten[10], R.D. Heuer[8], M.D. Hildreth[8], J.C. Hill[5], S.J. Hillier[1], P.R. Hobson[25], R.J. Homer[1], A.K. Honma[28,a], D. Horváth[32,c], K.R. Hossain[30], R. Howard[29], P. Hüntemeyer[27], D.E. Hutchcroft[5], P. Igo-Kemenes[11], D.C. Imrie[25], M.R. Ingram[16], K. Ishii[24], A. Jawahery[17], P.W. Jeffreys[20], H. Jeremie[18], M. Jimack[1], A. Joly[18], C.R. Jones[5], G. Jones[16], M. Jones[6], U. Jost[11], P. Jovanovic[1], T.R. Junk[8], D. Karlen[6], V. Kartvelishvili[16], K. Kawagoe[24], T. Kawamoto[24], P.I. Kayal[30], R.K. Keeler[28], R.G. Kellogg[17], B.W. Kennedy[20], J. Kirk[29], A. Klier[26], S. Kluth[8], T. Kobayashi[24], M. Kobel[10], D.S. Koetke[6], T.P. Kokott[3], M. Kolrep[10], S. Komamiya[24], T. Kress[11], P. Krieger[6], J. von Krogh[11], P. Kyberd[13], G.D. Lafferty[16], R. Lahmann[17], W.P. Lai[19], D. Lanske[14], J. Lauber[15], S.R. Lautenschlager[31], J.G. Layter[4], D. Lazic[22], A.M. Lee[31], E. Lefebvre[18], D. Lellouch[26], J. Letts[12], L. Levinson[26], S.L. Lloyd[13], F.K. Loebinger[16], G.D. Long[28], M.J. Losty[7], J. Ludwig[10], A. Macchiolo[2], A. Macpherson[30], M. Mannelli[8], S. Marcellini[2], C. Markus[3], A.J. Martin[13], J.P. Martin[18], G. Martinez[17], T. Mashimo[24], P. Mättig[3], W.J. McDonald[30], J. McKenna[29], E.A. Mckigney[15], T.J. McMahon[1], R.A. McPherson[8], F. Meijers[8], S. Menke[3], F.S. Merritt[9], H. Mes[7], J. Meyer[27], A. Michelini[2], G. Mikenberg[26], D.J. Miller[15], A. Mincer[22,e], R. Mir[26], W. Mohr[10], A. Montanari[2], T. Mori[24], M. Morii[24], U. Müller[3], S. Mihara[24], K. Nagai[26], I. Nakamura[24], H.A. Neal[8], B. Nellen[3], R. Nisius[8], S.W. O'Neale[1], F.G. Oakham[7], F. Odorici[2], H.O. Ogren[12], A. Oh[27], N.J. Oldershaw[16], M.J. Oreglia[9], S. Orito[24], J. Pálinkás[33,d], G. Pásztor[32], J.R. Pater[16], G.N. Patrick[20], J. Patt[10], M.J. Pearce[1], R. Perez-Ochoa8, S. Petzold[27], P. Pfeifenschneider[14], J.E. Pilcher[9], J. Pinfold[30], D.E. Plane[8], P. Poffenberger[28], B. Poli[2], A. Posthaus[3], D.L. Rees[1], D. Rigby[1], S. Robertson[28], S.A. Robins[22], N. Rodning[30], J.M. Roney[28], A. Rooke[15], E. Ros[8], A.M. Rossi[2], P. Routenburg[30], Y. Rozen[22], K. Runge[10], O. Runolfsson[8], U. Ruppel[14], D.R. Rust[12], R. Rylko[25], K. Sachs[10], T. Saeki[24], E.K.G. Sarkisyan[23], C. Sbarra[29], A.D. Schaile[34], O. Schaile[34], F. Scharf[3], P. Scharff-Hansen[8], P. Schenk[34], J. Schieck[11], P. Schleper[11], B. Schmitt[8], S. Schmitt[11], A. Schöning[8], M. Schröder[8], H.C. Schultz-Coulon[10], M. Schumacher[3], C. Schwick[8], W.G. Scott[20], T.G. Shears[16], B.C. Shen[4], C.H. Shepherd-Themistocleous[8],

P. Sherwood[15], G.P. Siroli[2], A. Sittler[27], A. Skillman[15], A. Skuja[17], A.M. Smith[8], G.A. Snow[17], R. Sobie[28], S. Söldner-Rembold[10], R.W. Springer[30], M. Sproston[20], K. Stephens[16], J. Steuerer[27], B. Stockhausen[3], K. Stoll[10], D. Strom[19], P. Szymanski[20], R. Tafirout[18], S.D. Talbot[1], S. Tanaka[24], P. Taras[18], S. Tarem[22], R. Teuscher[8], M. Thiergen[10], M.A. Thomson[8], E. von Törne[3], S. Towers[6], I. Trigger[18], Z. Trócsányi[33], E. Tsur[23], A.S. Turcot[9], M.F. Turner-Watson[8], P. Utzat[11], R. Van Kooten[12], M. Verzocchi[10], P. Vikas[18], E.H. Vokurka[16], H. Voss[3], F. Wäckerle[10], A. Wagner[27], C.P. Ward[5], D.R. Ward[5], P.M. Watkins[1], A.T. Watson[1], N.K. Watson[1], P.S. Wells[8], N. Wermes[3], J.S. White[28], B. Wilkens[10], G.W. Wilson[27], J.A. Wilson[1], G. Wolf[26], T.R. Wyatt[16], S. Yamashita[24], G. Yekutieli[26], V. Zacek[18], D. Zer-Zion[8]

[1]School of Physics and Space Research, University of Birmingham, Birmingham B15 2TT, UK
[2]Dipartimento di Fisica dell' Università di Bologna and INFN, I-40126 Bologna, Italy
[3]Physikalisches Institut, Universität Bonn, D-53115 Bonn, Germany
[4]Department of Physics, University of California, Riverside CA 92521, USA
[5]Cavendish Laboratory, Cambridge CB3 0HE, UK
[6] Ottawa-Carleton Institute for Physics, Department of Physics, Carleton University, Ottawa, Ontario K1S 5B6, Canada
[7]Centre for Research in Particle Physics, Carleton University, Ottawa, Ontario K1S 5B6, Canada
[8]CERN, European Organisation for Particle Physics, CH-1211 Geneva 23, Switzerland
[9]Enrico Fermi Institute and Department of Physics, University of Chicago, Chicago IL 60637, USA
[10]Fakultät für Physik, Albert Ludwigs Universität, D-79104 Freiburg, Germany
[11]Physikalisches Institut, Universität Heidelberg, D-69120 Heidelberg, Germany
[12]Indiana University, Department of Physics, Swain Hall West 117, Bloomington IN 47405, USA
[13]Queen Mary and Westfield College, University of London, London E1 4NS, UK
[14]Technische Hochschule Aachen, III Physikalisches Institut, Sommerfeldstrasse 26-28, D-52056 Aachen, Germany
[15]University College London, London WC1E 6BT, UK
[16]Department of Physics, Schuster Laboratory, The University, Manchester M13 9PL, UK
[17]Department of Physics, University of Maryland, College Park, MD 20742, USA
[18]Laboratoire de Physique Nucléaire, Université de Montréal, Montréal, Quebec H3C 3J7, Canada
[19]University of Oregon, Department of Physics, Eugene OR 97403, USA
[20]Rutherford Appleton Laboratory, Chilton, Didcot, Oxfordshire OX11 0QX, UK
[22]Department of Physics, Technion-Israel Institute of Technology, Haifa 32000, Israel
[23]Department of Physics and Astronomy, Tel Aviv University, Tel Aviv 69978, Israel
[24]International Centre for Elementary Particle Physics and Department of Physics, University of Tokyo, Tokyo 113, and Kobe University, Kobe 657, Japan
[25]Brunel University, Uxbridge, Middlesex UB8 3PH, UK
[26]Particle Physics Department, Weizmann Institute of Science, Rehovot 76100, Israel
[27]Universität Hamburg/DESY, II Institut für Experimental Physik, Notkestrasse 85, D-22607 Hamburg, Germany
[28]University of Victoria, Department of Physics, P O Box 3055, Victoria BC V8W 3P6, Canada
[29]University of British Columbia, Department of Physics, Vancouver BC V6T 1Z1, Canada

[30]University of Alberta, Department of Physics, Edmonton AB T6G 2J1, Canada
[31]Duke University, Dept of Physics, Durham, NC 27708-0305, USA
[32]Research Institute for Particle and Nuclear Physics, H-1525 Budapest, P O Box 49, Hungary
[33]Institute of Nuclear Research, H-4001 Debrecen, P O Box 51, Hungary
[34]Ludwigs-Maximilians-Universität München, Sektion Physik, Am Coulombwall 1, D-85748 Garching, Germany

[a] and at TRIUMF, Vancouver, Canada V6T 2A3
[b] and Royal Society University Research Fellow
[c] and Institute of Nuclear Research, Debrecen, Hungary
[d] and Department of Experimental Physics, Lajos Kossuth University, Debrecen, Hungary
[e] and Department of Physics, New York University, NY 1003, USA

1 Introduction

The production of heavy quarks in the decay of the Z^0 boson and their hadronisation have been the subject of considerable interest over the last few years. In particular the fractions with which the Z^0 boson decays into quark pairs of flavour q have been studied extensively in $Z^0 \to b\overline{b}$ decays [1–4], in $Z^0 \to c\overline{c}$ decays [5–8] and in light flavour events [9]. The fraction of $b\overline{b}$ events in Z^0 decays has been measured with very good precision. To achieve this goal, very efficient and pure bottom tagging methods have been developed, resulting in samples of events that are nearly free of non-bottom backgrounds. Significantly fewer and less precise measurements exist of the equivalent quantity for $c\overline{c}$ events or for light flavour events. In particular the selection of a pure $c\overline{c}$ sample has met with many difficulties, and the efficiencies and purities achieved by charm tags are inferior to those for bottom tags. The reason for this is that charmed hadrons are lighter and shorter lived than bottom hadrons, and are similar enough to most light hadrons to make a separation very difficult. However, the precise knowledge of the partial widths for different flavours constitutes an important test of the predictions of the Standard Model, since in lowest-order Born approximation the partial Z^0 decay width to $q\overline{q}$, $\Gamma_{q\overline{q}}$, is related to the coupling constants of the vector and axial vector current, g_V^q and g_A^q:

$$\Gamma_{q\overline{q}} = N_c^q \, \frac{G_\mu m_Z^3}{6\pi\sqrt{2}}((g_V^q)^2 + (g_A^q)^2) \ . \qquad (1)$$

Here G_μ is the Fermi decay constant and m_Z the Z^0 mass. The factor $N_c^q = 3$ denotes the number of colours. Higher order electroweak and QCD corrections to the Z^0 propagator and $q\overline{q}$ vertex that modify $\Gamma_{q\overline{q}}$ essentially cancel in the ratio $\Gamma_{q\overline{q}}/\Gamma_{had}$ except in the case of $Z^0 \to b\overline{b}$, where a small dependence on the Higgs mass and on the precise value of the top quark mass is introduced. The ratio $\Gamma_{q\overline{q}}/\Gamma_{had}$ therefore is the preferred measurable quantity, for which precise predictions exist in the context of the Standard Model for the quark flavours u,d,s and c, almost independent of unknown quantities.

In this paper a measurement of the fraction of primary $c\overline{c}$ pairs produced in the decays of Z^0 bosons is presented. At the same time the hadronisation fractions $f(c \to D^{*+}X)$ and $f(b \to D^{*+}X)$ are measured. The analysis is based on the identification of charged $D^{*\pm}$ mesons, electrons and muons.

The hadronisation fractions $f(c \to D^{*+}X)$ and $f(b \to D^{*+}X)$ are measured using a double tagging technique. To determine $f(c \to D^{*+}X)$, charged $D^{*\pm}$ mesons are sought in both event hemispheres[1]. The hadronisation fraction $f(b \to D^{*+}X)$ is determined in events tagged by a hard lepton in one hemisphere and a $D^{*\pm}$ in the other hemisphere. Comparing the number of such double tagged events with the number of singly reconstructed $D^{*\pm}$ mesons or leptons, the hadronisation fractions can be extracted with minimal model dependence and without explicit knowledge of the $D^{*\pm}$ or lepton reconstruction efficiencies.

The ratio of the charm partial width to the total hadronic width, $\Gamma_{c\overline{c}}/\Gamma_{had}$, is determined from the hadronisation fraction $f(c \to D^{*+}X)$ and from a measurement of the total production rate of $D^{*\pm}$ mesons in $Z^0 \to c\overline{c}$ events, $\Gamma_{c\overline{c}}/\Gamma_{had} \cdot f(c \to D^{*+}X)$. This rate is measured in this paper using a particularly well understood $D^{*\pm}$ decay mode, the decay[2] $D^{*+} \to D^0\pi^+, D^0 \to K^-\pi^+$.

Both the measurement of the hadronisation fraction and the measurement of $\Gamma_{c\overline{c}}/\Gamma_{had}$ rely heavily on the reconstruction of D^{*+} mesons using two different techniques. Therefore the

[1]The plane separating the two hemispheres in an event is defined perpendicular to the thrust axis of the event.

[2]Charge conjugation is assumed throughout this paper.

discussions in the first part of the paper concentrate on these technical aspects of the analysis. In the first technique described in section 4 the D^{*+} mesons are identified in a number of different decay channels by reconstructing all charged decay products. Since a significant contribution to the D^{*+} sample is from bottom hadron decays, a method has been developed to separate the different sources and is discussed in some detail. The second method of D^{*+} reconstruction is described next. It is a much more inclusive method, where only the pion in the decay $D^{*+} \to D^0\pi^+$ is used as the tag for the D^{*+}. In the last part of the section the tagging of $Z^0 \to b\overline{b}$ events using leptons is summarised.

In the second part of the paper the different measurements are presented. In section 5 the determination of the total rate of D^{*+} production in hadronic $Z^0 \to c\overline{c}$ decays is described. This is followed in section 6 by a presentation of the double tagging technique used to measure the hadronisation fractions for both bottom and charm events. Finally the results are combined to derive the relative partial width $\Gamma_{c\overline{c}}/\Gamma_{\mathrm{had}}$. The results reported in this paper supersede the ones given in [7], and complement the measurement of $\Gamma_{c\overline{c}}/\Gamma_{\mathrm{had}}$ reported in [8].

2 Analysis Principle

The main goal of this analysis is the measurement of the hadronisation fractions $f(c \to D^{*+}X)$ and $f(b \to D^{*+}X)$ and of $\Gamma_{c\overline{c}}/\Gamma_{\mathrm{had}}$. A double tagging technique is used to minimise model dependencies. However, because charm tags are rather inefficient a full double tag, where the same tag is applied to both hemispheres of the event, cannot be used. Instead two different charm tags are applied, one, which is pure, but has a comparatively small efficiency; and the other, which is more efficient, but less pure. The general strategy for the measurement of the hadronisation fractions is that a charm or bottom enriched sample is selected by applying the high purity charm or bottom tag to one hemisphere of the event, and then searching for D^{*+} mesons in the opposite hemisphere using the more efficient, less pure tag. Neglecting for simplicity any background from other flavours, the number of events of flavour q is given by

$$N_{\mathrm{tag1}} \sim \frac{\Gamma_{q\overline{q}}}{\Gamma_{\mathrm{had}}} f(q \to D^{*+}X)\, \epsilon_{\mathrm{tag1}} \;, \tag{2}$$

where ϵ_{tag1} is the efficiency to select an event of flavour q using the pure tag. The number of events, where a D^{*+} mesons is simultaneously identified in the second hemisphere, is given by

$$\begin{aligned} N_{\mathrm{tag1\,tag2}} &\sim \frac{\Gamma_{q\overline{q}}}{\Gamma_{\mathrm{had}}} f(q \to D^{*+}X)\, \epsilon_{\mathrm{tag1}} \times f(q \to D^{*+}X)\, \epsilon_{\mathrm{tag2}} \\ &= N_{\mathrm{tag1}} \times f(q \to D^{*+}X)\, \epsilon_{\mathrm{tag2}} \;. \end{aligned} \tag{3}$$

Here ϵ_{tag2} is the efficiency to tag a D^{*+} mesons using the second, efficient, tag in the flavour tagged sample. From the ratio of the number of double tagged events to the number of single tagged events the hadronisation fraction $f(q \to D^{*+}X)$ can be measured essentially without further assumptions or inputs. In this analysis the high purity flavour tags are an exclusive D^{*+} tag for $Z^0 \to c\overline{c}$ events, and a lepton tag for $Z^0 \to b\overline{b}$ events. The D^{*+} tag, applied to the sample of flavour tagged events, is based on a very inclusive method of identifying D^{*+} mesons using only the pion from the decay $D^{*+} \to D^0\pi^+$.

Significant backgrounds however exist from other than the desired flavours. In addition the efficiency to find a D^{*+} meson in the flavour tagged sample is not independent of the flavour tag itself. Background is particularly important in the case where the flavour tag is the charm tag. A significant part of the sample of D^{*+} mesons originates from $Z^0 \to b\overline{b}$ events, and also non-negligible contributions from combinatorial background events are found. The charm tagged sample is selected by fully reconstructing D^{*+} mesons that decay into a particular final state K^-Y with a branching ratio $\mathcal{B} = B(D^{*+} \to D^0\pi^+)\ B(D^0 \to K^-Y)$. The number of such events, $N_{D^{*+}}$, is given by

$$N_{D^{*+}} = 2N_{had} \cdot \sum_{q=b,c} (\frac{\Gamma_{q\overline{q}}}{\Gamma_{had}} f_q\, f\,(q \to D^{*+}X)\ \mathcal{B}\ \epsilon^q_{D^{*+}}) + N^{bgd}. \quad (4)$$

Here, N_{had} is the number of hadronic Z^0 decays used, $\Gamma_{q\overline{q}}/\Gamma_{had}$ is the relative partial width for a Z^0 to decay into a quark-antiquark pair of flavour q, f_q is the fraction of events with flavour q in the sample, $\epsilon^q_{D^{*+}}$ is the efficiency to reconstruct a D^{*+} meson in a $q \to D^{*+}$ hemisphere, and N_{bgd} is the number of background events in the sample. The fractions f_q satisfy the condition $f_c + f_b = 1$.

In this sample of flavour tagged events D^{*+} mesons are sought in the opposite hemisphere using the inclusive D^{*+} reconstruction. Background in the sample is reduced by requiring that the two D^{*+} candidates have opposite charges. The contribution from $b \to D^{*+}$ decays is further reduced since some of the bottom hadrons will have mixed before decaying into a D^{*+} meson. The number of double tagged events is therefore given by

$$N_{D^*\pi} = (N_{D^{*+}} - N^{bgd}) \cdot \left[f_c\, f\,(c \to D^{*+}X)\ \epsilon^c_{D^*\pi} + f_b\ (1-\chi_{eff})\ f\,(b \to D^{*+}X)\ \epsilon^b_{D^*\pi} \right] \cdot \mathcal{B}_* + N^{bgd}_{D^*\pi}\ , \quad (5)$$

where $\mathcal{B}_* = B(D^{*+} \to D^0\pi^+)$, $\epsilon^q_{D^*\pi}$ is the efficiency for tagging a D^{*+} meson using the inclusive tagging method in a $Z^0 \to q\overline{q}$ event, when a D^* meson has been identified in the opposite hemisphere, and χ_{eff} is an effective B^0–$\overline{B}^0$ mixing parameter applicable to the selected sample of events. It is interesting to note that eq. 5 does not depend on the efficiency of the high purity flavour tag, but only on the efficiency of reconstructing a D^{*+} meson inclusively.

The number of double tagged events given in equation 5 is proportional to both $f\,(c \to D^{*+}X)$ and to $f\,(b \to D^{*+}X)$. To separate the components the analysis is done twice, once as shown in eq. 5 in a charm enriched sample, tagged by the presence of D^{*+} mesons, and once in a bottom enriched sample, selected through hard leptons. The latter analysis is mostly sensitive to $f\,(b \to D^{*+}X)$, the former to $f\,(c \to D^{*+}X)$. By fitting the two samples simultaneously both hadronisation fractions are determined.

The charm partial width, $\Gamma_{c\overline{c}}/\Gamma_{had}$, is determined from the measured hadronisation fraction $f\,(c \to D^{*+}X)$ and from the total rate with which D^{*+} mesons are produced in $Z^0 \to c\overline{c}$ decays, $\Gamma_{c\overline{c}}/\Gamma_{had}\, f\,(c \to D^{*+}X)$. This is measured using a particularly well understood D^{*+} decay mode, $D^{*+} \to D^0\pi^+, D^0 \to K^-\pi^+$, which facilitates the source separation and the background subtraction. The only quantity which is not measured in this analysis, but has to be taken from external sources, is the branching ratio $B(D^{*+} \to D^0\pi^+)$.

3 The OPAL Detector and Event Selection

A detailed description of the OPAL detector can be found elsewhere [10]. This analysis relies heavily on the precise reconstruction of charged particle tracks and primary and secondary vertices in the event. This is achieved using a combination of two layers of a high precision silicon micro-vertex detector, installed nearest to the primary interaction point, and a system of large-volume gas-filled drift chambers which combine excellent spatial resolution with very good particle identification capabilities via the measurement of the specific energy loss of tracks.

The whole central tracking system is immersed in a magnetic field of 0.435 T, oriented along the direction of the electron beam. These central tracking detectors are surrounded by both electromagnetic and hadronic calorimeters with good energy resolution, providing nearly hermetic coverage over the full solid angle, and by a system of muon chambers on the outside of the detector.

Hadronic Z^0 decays are selected based on the number of reconstructed charged tracks and the energy deposited in the calorimeter [11]. The total hadronic event selection efficiency is found to be $(98.7 \pm 0.4)\%$. The selection slightly changes the flavour composition of the sample. This flavour bias is found to be less than 0.1% [4]. The analysis uses an initial sample of 4 374 410 hadronic decays of the Z^0 collected with the OPAL detector between 1990 and 1995.

Jets are reconstructed in the events by the cone jet finder [12] with a cone radius, R_{cone}, set to 0.7, and a minimum cone energy of at least 5 GeV. Events are only accepted if at least two jets are reconstructed. To ensure that the event is mostly contained in the sensitive detector volume, the absolute value of the cosine of the polar angle of the thrust axis with respect to the beam direction, $|\cos\theta_{\mathrm{thrust}}|$, has to be smaller than 0.9.

Tracks are used in the reconstruction if they pass loose track quality cuts requiring $|d_0| < 0.5$ cm, $|z_0| < 20$ cm, $p_{xy} > 0.250$ GeV and $n_{\mathrm{CJ}} > 40$. Here d_0 is the distance of closest approach between the primary vertex and the track measured in the plane perpendicular to the beam, z_0 the distance along the beam at this point, p_{xy} the momentum in the plane perpendicular to the beam, and n_{CJ} the number of hits on the track which are reconstructed in the main tracking chamber. The primary vertex in a collision is reconstructed from the charged tracks in the event and constrained by the known average position and spread of the e^+e^- interaction point.

Hadronic decays of the Z^0 have been simulated using the JETSET 7.4 Monte Carlo model [13] with parameters tuned to the data [14]. A sample of approximately 10 million simulated events was available for this analysis. In all samples heavy quark fragmentation was implemented using the Peterson model [15] with fragmentation parameters determined from LEP data [16]. All samples have been passed through a detailed simulation of the OPAL detector [17] before being analysed using the same programs as for data.

4 Heavy Flavour Tagging Techniques

Three different tagging techniques are employed to identify $Z^0 \to c\bar{c}$ and $Z^0 \to b\bar{b}$ events. The charm tags are based on the exclusive reconstruction of charged D^{*+} mesons (called "exclusive tag" in the following) in five different decay chains, or on a more inclusive D^{*+} reconstruction (called "inclusive tag" in the following). Bottom events are identified through the presence of an electron or a muon with large momentum and large transverse momentum relative to the direction of the jet containing the lepton. In this section the different tagging methods are described in some detail. Particular emphasis is placed on the method used to separate the contributions to the samples tagged by the different methods, where large backgrounds are present, and on the systematic errors connected with this source separation method. Very similar techniques have been used in previous OPAL publications for charm tags [7,18] and the bottom tag using leptons [4,19].

4.1 The Exclusive Charm Tag

The exclusive charm tag is based on the reconstruction of charged D^{*+} mesons in five different decay channels:

$$
\begin{array}{lll}
D^{*+} \to D^0\pi^+ & & \\
& \hookrightarrow K^-\pi^+ & \text{“3-prong”} \\
& \hookrightarrow K^-e^+\nu_e & \text{“electron”} \\
& \hookrightarrow K^-\mu^+\nu_\mu & \text{“muon”} \\
& \hookrightarrow K^-\pi^+\pi^0 & \text{“satellite”} \\
& \hookrightarrow K^-\pi^+\pi^-\pi^+ & \text{“5-prong”}
\end{array}
$$

In the following the electron and the muon channel are collectively referred to as “semileptonic”. No attempt is made to reconstruct the π^0 in the satellite channel, or the neutrino in the two semileptonic channels. Electrons are identified based on their energy loss in the jet chamber and the energy deposition in the electromagnetic calorimeter. An artificial neural network trained on simulated events is used to perform the selection [20]. Muon candidates are identified by associating tracks found in the central tracking system with tracks in the outer muon chambers [21].

In each channel a D^0 candidate is formed by combining an appropriate number of tracks, corresponding to the number of charged decay products in the chosen decay mode, assigning one to be a kaon, the rest to be pions or leptons, and calculating the invariant mass, M_0, of the set of tracks. Candidates are selected if the tracks assigned to the decay products have the correct charges, and if the reconstructed mass lies within the expected range, defined by the mass resolution in the different channels. The exact values are given in table 1. After adding a further track as a candidate for the pion in the D^{*+} decay the combined mass, M_*, is calculated and the candidate is selected if the mass difference $\Delta M = M_* - M_0$ is within given limits. Note that in cases where not all particles from the particular decay are reconstructed, the masses M_0 or M_* do not correspond to the physical particle masses of the D^0 or D^{*+} mesons, respectively.

For candidates with $x_{D^{*+}} = E^{\text{cand}}_{D^{*+}}/E_{\text{beam}} < 0.5$ the particle identification power of the OPAL detector is used to enrich the sample in true kaons. A probability $W^{KK}_{dE/dx}$, that the difference between the measured specific energy loss, dE/dx, determined for a track of momentum p, and the dE/dx value expected at that momentum for a kaon, is compatible with the kaon particle hypothesis, is calculated. A candidate track has to have a probability of at least 2% to be accepted as a kaon candidate. To ensure a reliable dE/dx measurement the number of charge measurements used in the dE/dx calculation, $n_{dE/dx}$, has to be at least 20.

Background in the sample is further reduced by cutting on the helicity angle θ^*, measured between the direction of the D^0 candidate in the laboratory frame and the direction of the kaon in the rest frame of the D^0 candidate. True kaons from D^0 decays are expected to be isotropically distributed in $\cos\theta^*$, while background displays pronounced peaks at $\cos\theta^* = -1$ and, particularly at low $x_{D^{*+}}$, at $\cos\theta^* = +1$.

To avoid multiple counting of events if more than one D^{*+} candidate is found, only one candidate per event is accepted. If more than one candidate is found per event a hierarchy is used to select the best one according to the signal purity. A 3-prong decay is preferred over a semileptonic one, which in turn is preferred over a satellite, and a 5-prong is selected last. For the semileptonic channel an electron is preferred over a muon candidate. If more than one candidate is found within one channel, the one with M_0 closest to its nominal value of $M_{D^0} = 1.864$ GeV [22] (1.6 GeV for the satellite) is selected.

A detailed list of the cuts used in the different channels is given in table 1. The reconstructed

cut	$x-$range	3-prong	semileptonic	satellite	5-prong
$x_{\mathrm{D}^{*+}}$		0.4–1.0	0.4–1.0	0.4–1.0	0.5–1.0
M_0 [GeV]	full	1.79–1.94	1.20–1.80	1.41–1.77	1.79-1.94
ΔM [GeV]	full	0.142–0.149	0.140–0.162	0.141–0.151	0.142–0.149
$W^{\mathrm{KK}}_{\mathrm{d}E/\mathrm{d}x}$	< 0.5	> 0.02			–
$n_{\mathrm{d}E/\mathrm{d}x}$	< 0.5	20			–
$\cos\theta^*$	< 0.5	-0.8–0.8			–
	> 0.5	-0.9–1.0			-0.9-1.0

Table 1: List of selection cuts used in the D^{*+} reconstruction. Note that both the scaled energy $x_{\mathrm{D}^{*+}}$ and the mass M_0 are effective quantities, calculated from the reconstructed tracks only. The exact meaning of the different quantities is explained in the text.

invariant mass spectra in all channels exhibit characteristic peaks at $\Delta M = 0.145$ GeV, close to the kinematic threshold of $\Delta M = m_\pi$. Clear signals are visible in all five channels, as shown in figure 1.

4.1.1 Partially Reconstructed D^{*+} Mesons

A significant fraction of the sample of selected D^{*+} mesons are only partially reconstructed. This is particularly obvious for events where neutral decay products are not identified, as is the case for the satellite or the semileptonic channels. Even in decays where all decay products are charged particles a fraction of events is present in the sample which are real D^{*+} decays, where however one or more tracks have been wrongly identified, or are missed completely. Such events are called "partially reconstructed D^{*+} mesons" if the slow pion of the $\mathrm{D}^{*+} \to \mathrm{D}^0\pi^+$ decay has been correctly found. These partially reconstructed D^{*+} mesons produce an enhancement in the ΔM spectrum very similar to the true signal. Only very few of these events are present in the 3-prong sample. They are much more important in the 5-prong tagged events, where a clear tail is visible in the ΔM distribution for values above 0.145 GeV (see figure 1(d)). Since such events originate from D^{*+} decays, they can still be used in the flavour tagging part of the analysis.

4.1.2 Combinatorial Background Estimation

The dominant background source is random combinations of tracks that pass the applied cuts. Only this combinatorial background component is considered background for the flavour tagging, and a method has been developed to subtract only this component from the sample of tagged events. The combinatorial background component is described by an estimator constructed entirely from data, optimised to exclude partially reconstructed D^{*+} candidates. It is constructed using a hemisphere mixing technique first introduced in [18]. The candidate for the pion in the $\mathrm{D}^{*+} \to \mathrm{D}^0\pi^+$ is taken from the opposite hemisphere relative to the rest of the candidate, and reflected through the origin, before being used in the calculation of the invariant mass. No requirements are placed on the charge of the D^{*+} background candidate, except that the total charge should be ± 1. The resulting distribution is used to define the shape of the background in ΔM. This method ensures that no true pions from the $\mathrm{D}^{*+} \to \mathrm{D}^0\pi^+$ decay are included in the estimator, and that the background shape does not exhibit any peak in the

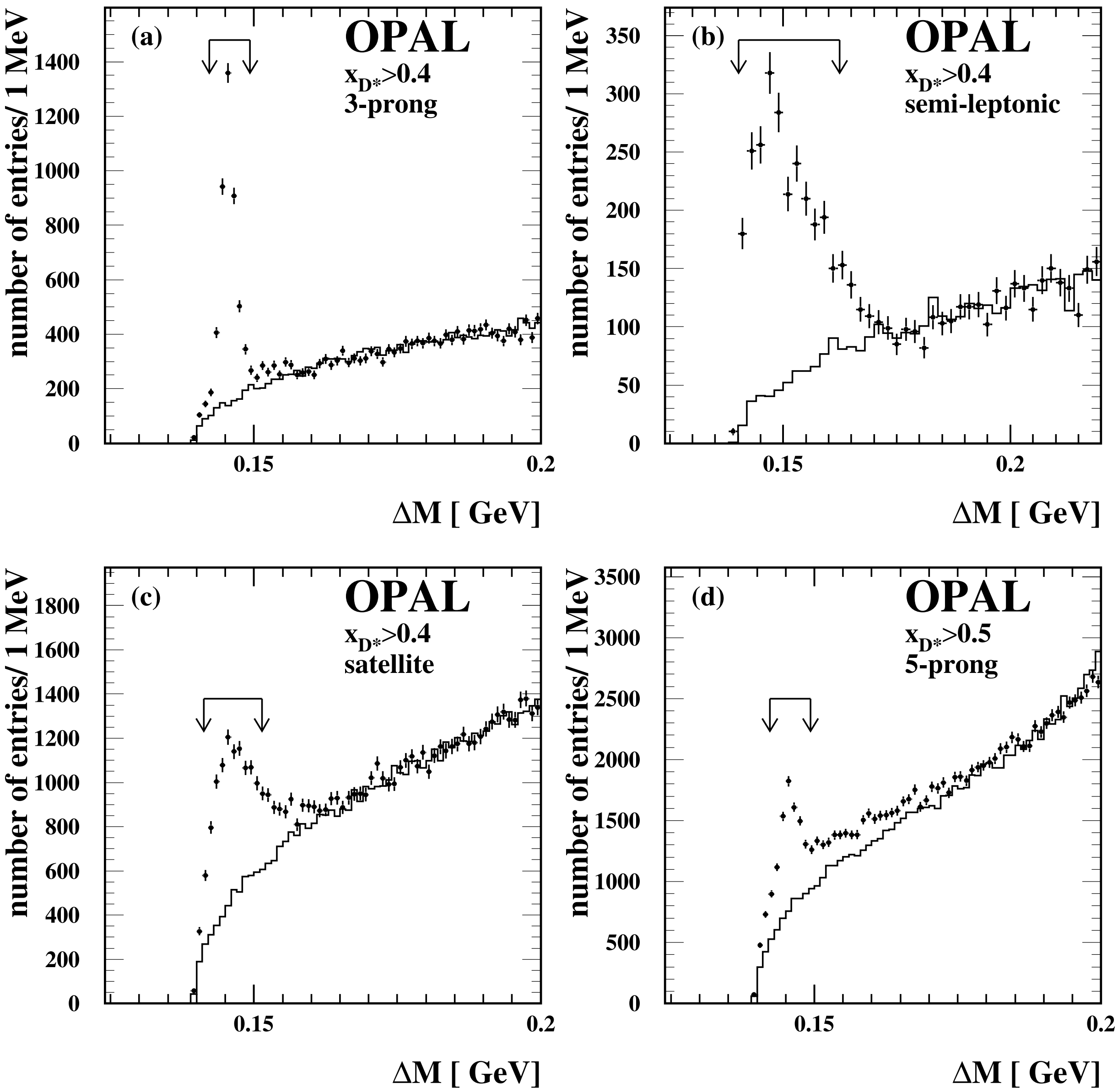

Figure 1: Distributions of the difference $\Delta M = M_{*} - M_{0}$ reconstructed in the four different D^{*+} channels. The arrows indicate the selected signal region. (a) 3-prong decay mode, (b) the two semileptonic modes combined, (c) the satellite decay mode, and (d) the 5-prong decay mode. The points with error bars are the signal candidates. Superimposed in each case (line histogram) are the background estimator distributions, normalised to the upper sidebands in ΔM.

decay channel	$x_{\mathrm{D}^{*+}}$ range	N_{cand}	N_{bgd}
3-prong	$0.4-1.0$	4649	1034 ± 28
semileptonic	$0.4-1.0$	2485	587 ± 23
satellite	$0.4-1.0$	10086	4537 ± 64
5-prong	$0.5-1.0$	9785	5208 ± 64
total		27 005	$11\,366\pm107$

Table 2: Number of observed candidates in the signal region and the estimated number of these which are background events. The error quoted for the background is the statistical error of the background sample, and does not contain systematic effects.

interesting ΔM region. The background distribution thus obtained is normalised to the candidate ΔM distribution in the range 0.18 GeV $< \Delta M <$ 0.20 GeV (0.19 GeV $< \Delta M <$ 0.22 GeV in the semileptonic channels). Monte Carlo studies have shown that this "reflected pion" estimator reliably models the shape of the combinatorial background in the sample. The number of candidates and the estimated number of background events are given for all channels in table 2.

4.1.3 Flavour Composition of the Exclusive $\mathrm{D}^{*\pm}$ Sample

The D^{*+} mesons contained in the tagged sample originate mostly in charm and bottom events, with a small contribution from events where a gluon splits into a pair of charm quarks. The latter is highly suppressed because of the high $x_{\mathrm{D}^{*+}}$ cut applied to the sample of selected events. Even more suppressed is the production of D^{*+} mesons from gluon splitting events into pairs of bottom quarks because of the large mass of the bottom quark. In this section the determination of the composition of the sample is described.

The composition of the tagged events is determined by applying three different bottom tags to the samples[3], and combining the results. Assuming for simplicity that no background from light flavours is present in the sample, the number of events tagged by a particular bottom tag is given by

$$N_{\mathrm{b-tag}} = (f_{\mathrm{b}}\ \mathcal{P}_{\mathrm{b}} + f_{\mathrm{c}}\ \mathcal{P}_{\mathrm{c}})\ N_{\mathrm{cand}}\ . \tag{6}$$

Here $f_{\mathrm{b}} = 1 - f_{\mathrm{c}}$ is the bottom (charm) fraction in the sample, and the $\mathcal{P}_{\mathrm{b,c}}$ are the probabilities that an event in which a D^{*+} meson has been identified is also tagged by the bottom tag. If these tagging probabilities are known, the bottom fraction can be calculated. The bottom tags are applied on a jet basis, both in the jet containing the exclusively reconstructed D^{*+} candidate (called the "D-jet"), and in the remaining highest energetic jet in the event (called the "secondary jet").

In practise additional backgrounds are present in the sample. The number of background events tagged with the different bottom tags and included in the sample is measured from data in independent background samples. For this a background sample for each tagging technique is prepared, the total number of events in the background sample is normalised to the number of background events measured, and the bottom tag is applied to this sample.

[3]The same method has been used in [7], where additional details may be found.

The three different bottom tagging techniques are based on lifetime information, on jet-shapes and on hemisphere charge information. The first two have been used in earlier OPAL publications [7,18], and are only briefly reviewed. The last one will be covered in more detail.

Lifetime information is reconstructed in both jets used in this analysis. Vertices are reconstructed inclusively as in [23], and a decay length significance d/σ is calculated, where d is the distance between the primary and the secondary vertex, constrained by the jet direction, and σ its error. Bottom events are identified by their large decay length significance values. The shape of the combinatorial background is estimated using the reflected pion technique discussed in section 4.1.2. The background estimator distribution is normalised to the sidebands in ΔM, and is subtracted from the candidate distributions.

Jet-shape information is used in the jet opposite the D-jet. The shapes are measured by a set of seven jet shape variables, which are defined in [7], and are combined using a neural net technique into one tag. The combinatorial background is estimated in data using a wrong charge technique, where background events are identified by the presence of a candidate with an unphysical charge combination of the decay products.

The third method uses the observation that the charge of the primary quark can be measured on a statistical basis using the hemisphere charge. Since the correlations between the charges of the D^{*+} mesons and the sign of the charge of the primary quark are opposite for bottom and for charm quarks, measuring the D^{*+} charge and the primary quark charge in the opposite hemisphere provides some separation between bottom and charm events. The hemisphere charge is determined from all tracks in the hemisphere according to

$$Q_{\mathrm{hem}} = \frac{\sum_i |p_i|^\kappa q_i}{\sum_i |p_i|^\kappa} \ , \tag{7}$$

where i runs over all tracks in a hemisphere, p_i is the momentum component along the thrust axis of track i in the hemisphere, and q_i is its charge. The exponent κ is a weighting factor which has been optimised using Monte Carlo simulation to be 0.4 for the purpose of flavour separation. Similar to the other two methods described a tagging efficiency $P_{\mathrm{q}}, \mathrm{q} = \mathrm{b}, \mathrm{c}$ is determined from Monte Carlo. The shape of the background in the hemisphere charge is estimated from events tagged in sidebands of the ΔM distributions, $\Delta M > 0.18$ GeV, in the D^{*+} sample.

In all three cases the tagging probabilities are taken from the Monte Carlo simulation. The final fit for the flavour composition is performed simultaneously with the information from all three methods. It is done separately for each exclusive channel considered, and in bins of the scaled energy $x_{\mathrm{D}^{*+}}$ of the candidate. The most significant contribution to the separation comes from the decay length significance analysis, which contributes with a weight of 0.41 from the D^{*+} hemisphere analysis, and 0.27 from the opposite hemisphere. The jet-shape analysis enters with a relative weight of 0.21, the hemisphere charge with 0.11. Distributions of the tagging variables are shown in figure 2. Combining all exclusive channels the charm fraction in the D^{*+} tagged sample, for the range of $x_{\mathrm{D}^{*+}}$ detailed in table 1, is determined to be

$$f_{\mathrm{c}}^{\mathrm{D}^{*+}} = 0.774 \pm 0.008 \ , \tag{8}$$

where the error quoted is purely statistical.

4.1.4 Contribution from $\mathrm{g} \rightarrow \mathrm{c\bar{c}}$

Small contributions to the signal are expected from the splitting of a gluon into a pair of charm quarks. This rate has been measured in [7,24], where the multiplicity of $\mathrm{c\bar{c}}$ pairs produced in

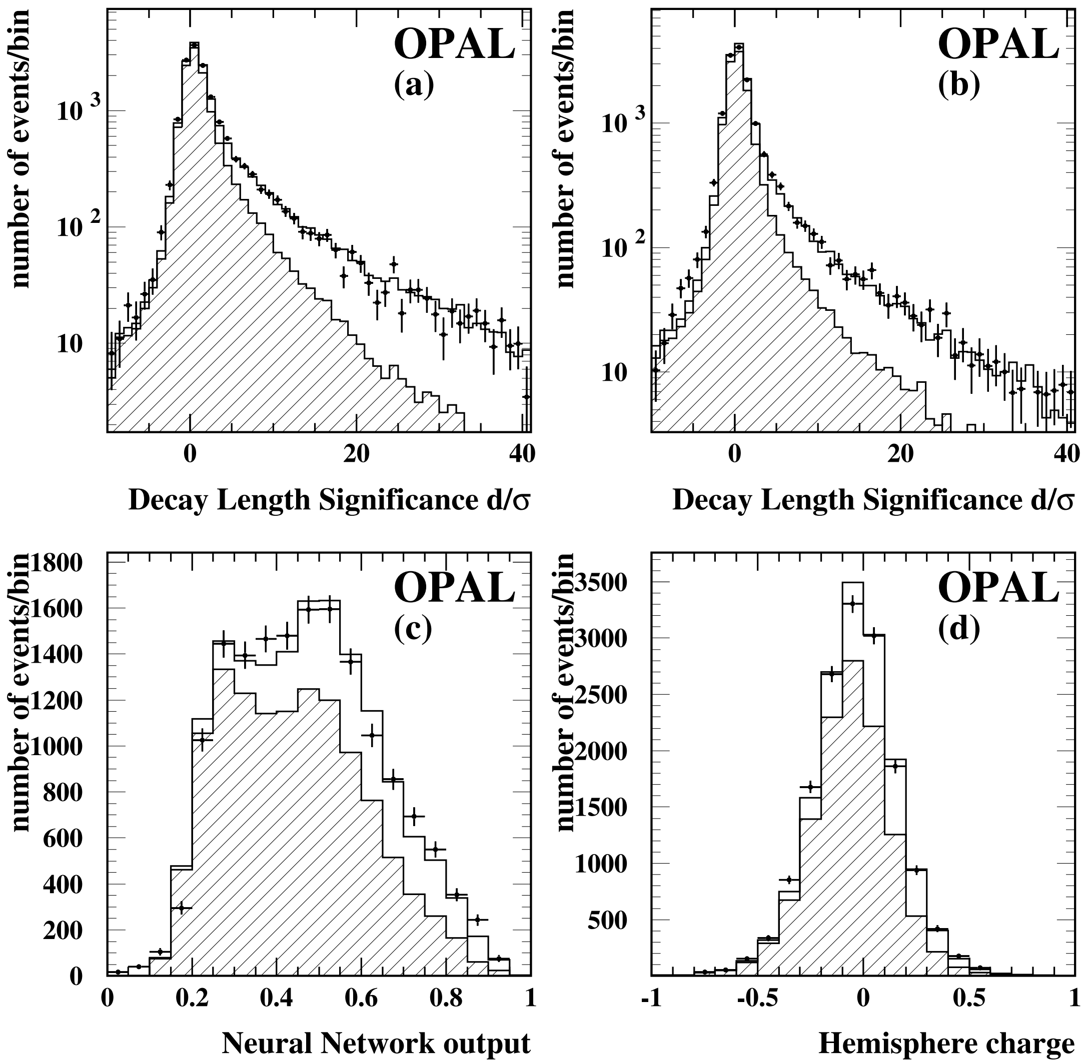

Figure 2: Distributions of the different tag-variables used in the flavour separation. Shown are the data distribution after background subtraction (points with error bars), the equivalent Monte Carlo distribution for all candidates (open histogram) and the predicted charm component (hatched histogram). Shown are the (a) decay length significance in the jet with the exclusive D^{*+} candidate; (b) decay length significance in the jet opposite the exclusive D^{*+} candidate; (c) distribution of the neural network based on jet-shape variables, and (d) distribution of the hemisphere charge.

hadronic decays of the Z^0 is found to be $\bar{n}_{g\to c\bar{c}} = 0.0238 \pm 0.0048$. Using Monte Carlo simulation the fraction of events from this source in the selected sample of events is estimated and, after normalising to the measured rate, subtracted from the tagged sample of D^{*+} events. The total contribution of these events to the exclusively tagged sample is found to be $(0.2 \pm 0.1)\%$, where the error quoted is only due to Monte Carlo statistics.

4.1.5 Systematic Errors of the Flavour Separation Method

A number of errors are introduced by the flavour separation method employed. The errors quoted are relative errors on the charm fraction in the sample.

- Detector resolution: The influence of the detector resolution on the tagging variables is studied in Monte Carlo by varying the resolutions in the tracking system by $\pm 10\%$ relative to values that optimally describe the data. The analysis is repeated and efficiencies are recalculated. The error quoted is the largest observed deviation in this study, and amounts to 0.6%.

- Background modelling: The distributions in the tagging variables for background events are taken from estimator distributions determined using data. Possible differences between the estimator and the true background distributions are studied using Monte Carlo simulations. The separation is repeated with the background distribution taken from Monte Carlo, and the differences are used as systematic errors. Similarly, errors in the determination of the normalisation of background in the sample will change the reconstructed b-fraction (and, since they are totally anti-correlated, the c fraction). This has been studied by varying the background within its total error. In total the error from these sources amounts to 1.7%.

- Detector response: Possible inhomogeneities of the detector response as a function of $\cos\theta$ are studied by repeating the flavour separation in bins of $\cos\theta$, and by comparing the results with the overall determination. No significant differences are found.

- Hemisphere correlations: Part of the flavour separation is done in the hemisphere opposite to the reconstructed D^{*+} mesons. Small correlations are expected to exist between the two hemispheres, which possibly might bias the measurement of the flavour composition. In the flavour separation these biases are taken into account by calculating the tagging efficiencies in bins of $x_{D^{*+}}$ as measured from the exclusive D candidate. The size of the bias is estimated by recalculating the tagging efficiencies in only one bin of $0.4 < x_{D^{*+}} < 1.0$, and repeating the analysis. This is done for all three tagging algorithms. The resulting error is 0.4%.

- Charm modelling: The jet-shape analysis is sensitive to the modelling of the response to charm events, which is taken from Monte Carlo simulation. Possible modelling problems are investigated by comparing the network output distribution in an unbiased sample of hadronic Z^0 decays in data and Monte Carlo. All observed differences are assumed to come from charm modelling problems, and a systematic error of 1% is calculated. The same method was used in [7].

- Charm and bottom multiplicity: The vertex finder employed is sensitive to the charged multiplicity from charm and bottom hadron decays in the sample. The multiplicity for heavy flavour decays in the Monte Carlo has been varied by reweighting simulated events, corresponding to the current experimental bounds of ± 0.2 tracks for charm decays, and ± 0.35 tracks for bottom decays [16]. Similarly the hemisphere charge technique is sensitive to the multiplicity, and its error is estimated using the same procedure. Overall this results in an error of 0.6% for charm and 0.5% for bottom.

- B hadron lifetime: The B hadron lifetime has been varied within its current experimental limits: In the D hemisphere the lifetimes of the different B species have been varied independently by ± 0.07 ps for the B^+, ± 0.08 ps for the B^0, and ± 0.12 ps for the $\mathrm{B_s}$ [22]. In the hemisphere opposite to the D meson, the mean B hadron lifetime of (1.549 ± 0.020)ps [22] has been used and changed within its error. The total error is found to be 0.7%.

- Charm lifetime: The lifetimes of the weakly-decaying charmed hadrons D^0 and D^+ has been varied independently by ± 0.004 ps for the D^0, and ± 0.015 ps for the D^+ [22], corresponding to a total error of 0.4%.

- $\mathrm{B}^0 - \overline{\mathrm{B}}^0$ mixing: Mixing of neutral B mesons changes the correlation between the charge of the quarks in the two hemispheres of the event. The hemisphere charge method is sensitive to the assumed value of the mixing through the bottom tagging efficiency. Two different mixing parameters have to be considered: the average B mixing in the hemisphere opposite the tagged D^{*+}, and the effective mixing in tagged D^{*+} events. The latter is different because the mixture of B mesons in D^{*+} tagged events is different from an unbiased sample. The derivation of this effective mixing is described later in this paper in section 6.2.2, and is determined with an error of $\pm 17\%$. Compared to this the error on the average mixing is very small and is neglected. Applied to the b/c separation this translates into an error of 0.3%.

- Fragmentation model: The fragmentation functions used in Monte Carlo simulation for heavy flavour events influence all three tagging algorithms. The Peterson [15] scheme is used for bottom and charm hadrons. To estimate the influence on the results the mean scaled energy of primary charm and bottom hadrons has been varied around their measured values of $\langle x_{\mathrm{b}} \rangle = 0.702 \pm 0.008$ and $\langle x_{\mathrm{D}^{*+}} \rangle = 0.510 \pm 0.009$, as suggested in [16], and the separation has been redone. This results in an error of 0.6%.

The final charm fraction in the D^{*+} tagged sample for the selected $x_{\mathrm{D}^{*+}}$ range is found to be

$$f_{\mathrm{c}}^{\mathrm{D}^{*+}} = 0.774 \pm 0.008 \pm 0.022 \ , \tag{9}$$

where the first error is statistical, the second one systematic.

4.2 The Inclusive Charm Tag

The second, more inclusive, charm tag relies on the very special kinematical properties of the decay $\mathrm{D}^{*+} \to \mathrm{D}^0 \pi^+$. Because of the small mass difference of only 145 MeV between the D^{*+} and the D^0 very little phase space is left for the pion. In the laboratory frame this pion, called the "slow pion" in the following, is emitted essentially in the direction of the D^{*+} meson, with a maximal transverse momentum p_t relative to the D^{*+} direction of flight of 39 MeV. A charm tag is constructed from this by looking for an enhancement in the density of tracks along the D^{*+} flight direction.

The fraction of slow pions from $\mathrm{c\overline{c}}$ events is enhanced by requiring:

- $1.0 \;\; \mathrm{GeV} < p_\pi < 3.0 \;\; \mathrm{GeV}$,

where p_π is the momentum of the pion candidate. Kaon and electron contamination in the slow pion candidate sample is reduced by using the particle identification power of the drift chamber in the OPAL detector, requiring

- $W^{\pi\pi}_{\mathrm{dE/dx}} \; > \; 0.02$,
- $n_{\mathrm{d}E/\mathrm{d}x} > 20$,

where $W^{\pi\pi}_{\mathrm{dE/dx}}$ is the $\mathrm{d}E/\mathrm{d}x$ probability for a pion, and $n_{\mathrm{d}E/\mathrm{d}x}$ the corresponding number of measurements used, as defined in section 4.1.

The flight direction of the D^{*+} meson is reconstructed inclusively by an iterative procedure. It uses the fact that decay products from heavy mesons are on average harder and more collimated than those from fragmentation tracks, leading on average to higher values of the rapidity[4] $y = (1/2)\log[(E+p_z)/(E-p_z)]$ with respect to flight direction of the D^{*+} meson. The decay products are selected by first grouping all tracks and unassociated neutral clusters in the event into jets using the cone algorithm, described in section 3. The jet axis is computed from all particles in the jet after removing the slow pion candidate itself. If tracks or clusters exist which have a rapidity measured relative to the direction of the jet, of less than 2.5, the one with the smallest rapidity is removed from the calculation, and the direction is recomputed. This procedure is repeated until all particles have a rapidity value above 2.5, or the number of tracks or clusters is less than two. In this case the original jet direction is used. The direction determined in this manner is used as an estimate of the D^{*+} flight direction. The resolution, measured as the width of the p_t^2 distribution at 50% of its maximal value, is found to be $\sigma(p_t) = 0.056$ GeV. The efficiency with which $\mathrm{D}^{*+} \to \mathrm{D}^0\pi^+$ decays are selected using this method is around 40% in $\mathrm{c\overline{c}}$ events, and around 20% in $\mathrm{b\overline{b}}$ events. A similar procedure was first introduced in [25].

4.3 The Bottom Tag

A pure sample of bottom events is selected using a lepton tag. This sample will be used in the measurement of $\mathrm{f}\,(\mathrm{b} \to \mathrm{D}^{*+}\mathrm{X})$ as the flavour tagged sample, and takes the place of the exclusive D^{*+} tag described earlier. Electrons and muons are identified as described in section 4.1. The sample is purified by requiring that electrons have a momentum larger than 2.0 GeV, and a transverse momentum relative to the jet direction larger than 1.1 GeV. Electrons are only reconstructed in the central region of the detector, if the polar angle is below $|\cos\theta| < 0.715$. Muons have to have a momentum above 3.0 GeV, a transverse momentum larger than 1.2 GeV and $|\cos\theta| < 0.9$. According to the Monte Carlo simulation this sample has a bottom purity of (89.90 ± 0.14)%. Of the remaining events 33% are from semileptonic charm decays, and 66% are misidentified leptons.

4.3.1 Systematic Errors of the Lepton Tag

The purity of the lepton identification is taken from Monte Carlo simulation. The following systematic errors have been investigated:

[4]The momentum p_z is measured relative to the jet axis. Charged particles are assumed to be pions, neutral particles photons.

- Detector resolution: The resolution of the tracking part of the detector is varied by 10%, resulting in an error on the purity of 0.1%.

- Bottom fraction in Z^0 decays: The fraction of $Z^0 \to b\bar{b}$ events in the Monte Carlo is re-weighted to the one measured by OPAL: $\Gamma_{b\bar{b}}/\Gamma_{had} = 0.2175 \pm 0.0022$ [4]. The error on the measurement is used to calculate the corresponding systematic error of 1.0%.

- Heavy flavour fragmentation: The fragmentation parameters in the Monte Carlo have been varied to change the mean scaled energy of charm and bottom hadrons around their experimental values of 0.702 ± 0.008 and 0.510 ± 0.009 respectively. The error on the bottom purity is 0.8%.

- Decay modelling: The momentum distribution of the lepton produced in a bottom or a charm decay influences the tagging efficiency. Following the recommendations in [16] this was studied by reweighting the distribution in the Monte Carlo to different models. Models used are ACCM, ISGW and ISGW**. The largest observed deviation is used as a systematic error, resulting in an error of 1.4%.

- Semileptonic branching ratios: The semileptonic branching ratios $B(b \to \ell)$ and $B(c \to \ell)$ have been measured at LEP. The spectra in B-decay are determined also at lower energy machines. The values recommended in [16] are used, and the Monte Carlo is re-weighted to these measured values. Systematic errors are derived from the errors on the branching ratios. The error on the purity is 0.3%.

- Hadronic background: Around 6% of the sample of tagged leptons are hadrons, which were misidentified. In [4], the error of the mistagging rate has been determined to be 9.3% in the electron sample, and 9.0% in the muon sample. This translates into an error of 0.6% of the bottom purity.

The total systematic error of the bottom purity in lepton tagged events is found to be 2.1%. Note that the knowledge of the lepton reconstruction efficiency is not required in this analysis, as discussed in section 2.

5 Production of D^{*+} Mesons in $Z^0 \to c\bar{c}$ and $Z^0 \to b\bar{b}$ Decays

In this part the total production rates $\Gamma_{c\bar{c}}/\Gamma_{had} \cdot f(c \to D^{*+}X)\, B(D^{*+} \to D^0\pi^+)\, B(D^0 \to K^-\pi^+)$ and $\Gamma_{b\bar{b}}/\Gamma_{had} \cdot f(b \to D^{*+}X)\, B(D^{*+} \to D^0\pi^+)\, B(D^0 \to K^-\pi^+)$ are determined. The results for $f(c \to D^{*+}X)$ is used later in the analysis to determine the relative partial width $\Gamma_{c\bar{c}}/\Gamma_{had}$. In addition the mean scaled energy of D^{*+} mesons in $Z^0 \to c\bar{c}$ events, $\langle x_{D^{*+}} \rangle_c$ is measured, and the total multiplicity of charged D^{*+} mesons in Z^0 decays is given.

The analysis is performed using the sample of fully reconstructed D^{*+} mesons in the 3-prong decay mode. To minimise the number of D^{*+} mesons not observed the $x_{D^{*+}}$-range for this part of the analysis has been extended to $x_{D^{*+}} = 0.2$. The reconstruction method is similar to the one described in the previous section for the exclusive charm tag. An important difference however is the treatment of the partially reconstructed D^{*+} decays. While previously they have been treated as signal for the purpose of tagging the primary event flavour, they are background for the determination of the total rate of D^{*+} meson production in this particular channel. Therefore the background subtraction is rediscussed in some detail, and a method of treating the contribution from such partially reconstructed decays is introduced.

5.1 Background Subtraction

Backgrounds for the purpose of the measurement of the production rate of D^{*+} mesons are combinatorial background and partially reconstructed decays of D^{*+} mesons. The former is determined with essentially the same procedure as described above, except that the combinatorial background, after having been normalised, is not simply subtracted, but is fitted using a simple parametrisation. The contribution from partially reconstructed D^{*+} decays is measured in the data with a special procedure. In this part of the analysis no requirement is made that only one candidate be found in the channel, unlike that for the sample of D^{*+} mesons used in the exclusive charm tag. This different treatment is possible since the 3-prong decay is very clean, and the number of partially reconstructed events is small.

The combinatorial background in the sample is determined as before from the reflected pion estimator. The ΔM distributions obtained using this estimator are normalised to the candidate ΔM distribution for 0.16 GeV $< \Delta M <$ 0.2 GeV. It is then parametrised using an empirical functional form

$$f(\Delta M) = A\,(\frac{1}{m_{\pi^+}}(\Delta M + B\,(\Delta M)^2))^C \;, \tag{10}$$

with A, B and C free parameters determined in the fit described below. The number of background events is determined in 16 bins of $x_{D^{*+}}$ between $x_{D^{*+}} = 0.2$ and 1.0, in the signal region 0.142 GeV $< \Delta M <$ 0.149 GeV. The mass difference distribution for the 3-prong sample only, with the result of the background fit superimposed, is shown in figure 3(a) for the $x_{D^{*+}}$ range between 0.2 and 1.0.

From Monte Carlo simulation about 8% of the signal, after subtracting the combinatorial background, actually come from partially reconstructed D^{*+} mesons. They are mostly products of the following decays: $D^0 \to K^-\pi^+\pi^0$ (4.3%), $D^0 \to K^-K^+$ (1.8%), $D^0 \to \pi^-\pi^+$ (0.7%), $D^0 \to \pi^-\pi^+\pi^0$ (0.5%) and $D^0 \to K^-\ell^+\nu$ (0.3%). The numbers in brackets indicate the predictions from the Monte Carlo simulation for the contribution to the full D^{*+} sample from each source.

Instead of using the Monte Carlo predictions the total contribution is measured in data in a simultaneous fit to the M_0 and the ΔM distributions of all candidate D^{*+} mesons. The M_0 distribution is examined for candidates where the mass difference ΔM is inside the tight signal region of 0.142 GeV $< \Delta M <$ 0.149 GeV, and no M_0 cut has been applied. Contributions from partially reconstructed D^{*+} mesons are in general characterised by a peak in the ΔM distribution at the position expected for correctly identified D^{*+} mesons, but no peak-like structure in the M_0 distribution at the position expected for true D^0 mesons. Therefore the difference between the number of reconstructed D^{*+} mesons as derived from the ΔM distribution and and from the M_0 distribution can be used as a measure of the fraction of partially reconstructed decays in the sample. A slight complication arises from the decay $D^0 \to K^-K^+$, which is expected to peak just below the nominal D^0 mass. Monte Carlo simulation is used to account for this.

The number of D^{*+} candidates is extracted from the M_0 mass spectrum using a fit. The combinatorial background is parametrised by an exponential function. The signal function has two contributions: the first describes the true 3-prong candidates, and is constructed from two gaussian functions, motivated from Monte Carlo simulation studies, with the second having three times the width and the same mean as the first. The second function parametrises

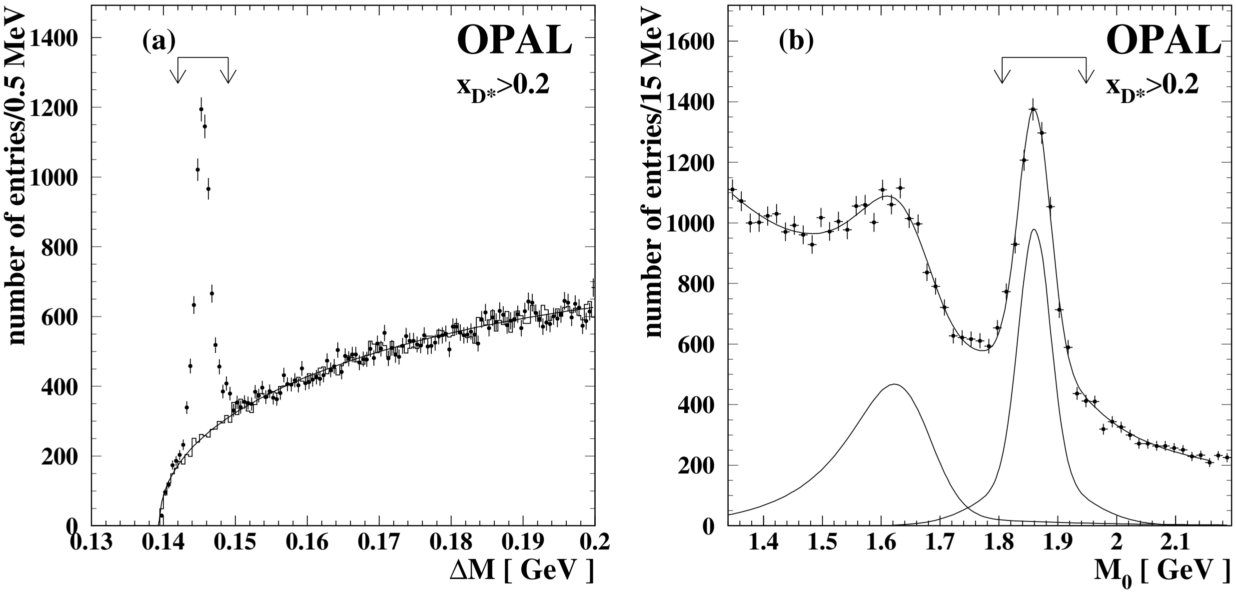

Figure 3: (a) Distribution of the mass difference $\Delta M = M_* - M_0$ reconstructed in the decay $D^{*+} \rightarrow D^0\pi^+$, $D^0 \rightarrow K^-\pi^+$. Superimposed is the background distribution obtained from the background estimator discussed in the text, and the result of the fit to this background estimator. The arrows indicate the selected signal region. (b) M_0 spectrum of D^{*+} candidates, with M_0 cut removed, and an additional ΔM cut applied. Shown are the data (points with error bars), the result of the fit as described in the text, and the two components from satellite and from fully reconstructed D^{*+} mesons, as obtained in the fit. The arrows indicate the selected signal region.

the contribution from partially reconstructed decays in the signal region. It is dominated by satellite decays which cluster below the expected D^0 mass of 1.865 GeV. As expected from the kinematics of this decay the mass distribution is approximately gaussian, with a significant tail towards smaller masses. It is parametrised by a gaussian convoluted with an exponential function. The decay constant in the exponential is fixed relative to the width of the gaussian function to the value obtained in the Monte Carlo. The other decays contributing to the partially reconstructed sample are described by an additional exponential function, added to the parametrisation of the satellite decay. This essentially adds a tail to the satellite function, which extends into the nominal D^0 mass region. Monte Carlo is used to estimate the contribution coming from the $D^0 \rightarrow K^-K^+$ decay, which is not described by the tail. The shapes of the different fit functions have been tested in Monte Carlo simulated events, and are found to provide a good description of the mass spectra. Because of the complicated fit function, and because the fraction of partially reconstructed decays varies only slowly with $x_{D^{*+}}$, this fit is done in four equal-sized bins of $x_{D^{*+}}$ between 0.2 and 1.0, instead of the 16 used in the ΔM fits. The number of D^{*+} mesons is obtained by integrating the signal function over the mass window 1.79 GeV $< M_0 <$ 1.94 GeV. The fraction of partially reconstructed D^{*+} events in this bin is then calculated from the difference between the number of signal events determined with this fit, and the sum of the number of signal candidates over the appropriate $x_{D^{*+}}$ bins found in the fit using the ΔM method. The M_0 spectrum for all candidates, with the results of the fit superimposed, is shown in figure 3(b).

Monte Carlo studies indicate that this method reliably reproduces the number of partially reconstructed D^{*+} mesons in the sample. The total contribution from all sources is predicted to amount to $(7.9\pm0.5)\%$, while the fit in the Monte Carlo sample measures this to be $(7.8\pm2.2)\%$. In the data the same procedure gives the contribution from partially reconstructed decays to be $(8.1\pm1.7)\%$, in excellent agreement. In total 8497 candidates are found, of which 3750 ± 24 are background events, where the error given is the statistical error from the fit.

5.2 Flavour Composition and Fragmentation Fits

The main contributions to the sample of tagged events are the same as described in section 4.1.3. The principal method for determining the flavour composition is the same as was described for the exclusive D^{*+} sample. The goal of this analysis is the determination of the absolute rate of D^{*+} production in charm and bottom decays. Therefore the observed number of D^{*+} mesons needs to be corrected for the reconstruction efficiency which can be done reliably only in the 3-prong sample. In addition knowing the efficiencies allows to constrain the shape of the fragmentation function to a particular shape. Previous studies [7, 8] have shown that the efficiency corrected fragmentation function in charm decays can be described well by the function of Peterson et al. [15].

The flavour separation is done in the $x_{D^{*+}}$ range $0.2 < x_{D^{*+}} < 1.0$, subdivided into 16 bins of $x_{D^{*+}}$. The charm and the bottom fragmentation functions are constrained to the Peterson shape by convoluting the analytical fragmentation function with the effects of the hadronisation as predicted by the JETSET 7.4 model. A simultaneous fit is then done using the mean scaled energy and the information from the flavour separation procedure. The normalisations for both bottom and charm decays and the Peterson parameters ε_c and ε_b are allowed to vary in the fit.

The efficiency of the D^{*+} reconstruction is calculated in bins of $x_{D^{*+}}$ separately for $Z^0\to b\overline{b}$ and for $Z^0\to c\overline{c}$ events in the Monte Carlo simulation. The efficiency is essentially constant as a function of $x_{D^{*+}}$, with a small step at $x_{D^{*+}} = 0.5$ due to the change in the $\mathrm{d}E/\mathrm{d}x$ and the $\cos\theta^*$ cuts. Typically it is $(25.0\pm0.6)\%$ for $x_{D^{*+}} < 0.5$, and $(30.0\pm0.5)\%$ for $x_{D^{*+}} > 0.5$, with the bottom and charm efficiencies being very similar.

Some of the tagged D^{*+} events are expected to come from gluon splitting. The OPAL measurement for the gluon splitting rate is used [7, 24], and the shape is taken from the Monte Carlo prediction as was done in [7]. The result of the separation is shown in figure 4, where the total efficiency-corrected yield, the charm component, the bottom component and the part from gluon splitting are shown.

Integrating the fitted fragmentation functions over the full $x_{D^{*+}}$ range the product branching ratio in charm events is found to be

$$\Gamma_{c\overline{c}}/\Gamma_{had}\cdot f\,(c\to D^{*+}X)\,B(D^{*+}\to D^0\pi^+)\,B(D^0\to K^-\pi^+) \;=\; (1.041\pm0.020)\times10^{-3}\ ,$$

where only the statistical error has been quoted. The χ^2 per degree of freedom is 1.28.

Though not directly needed in this analysis the same fit returns information about the production of D^{*+} mesons in $Z^0\to b\overline{b}$ events, the total D^{*+} multiplicity, and the hardness of the D^{*+} fragmentation function in charm decays. In bottom events the product branching ratio is determined to be

$$\Gamma_{b\overline{b}}/\Gamma_{had}\cdot f\,(b\to D^{*+}X)\,B(D^{*+}\to D^0\pi^+)\,B(D^0\to K^-\pi^+) \;=\; (1.334\pm0.049)\times10^{-3}\ .$$

The errors quoted are only statistical. The correlation between the total production rate in $Z^0\to c\overline{c}$ and in $Z^0\to b\overline{b}$ events is found to be -23%. Adding the predicted gluon component,

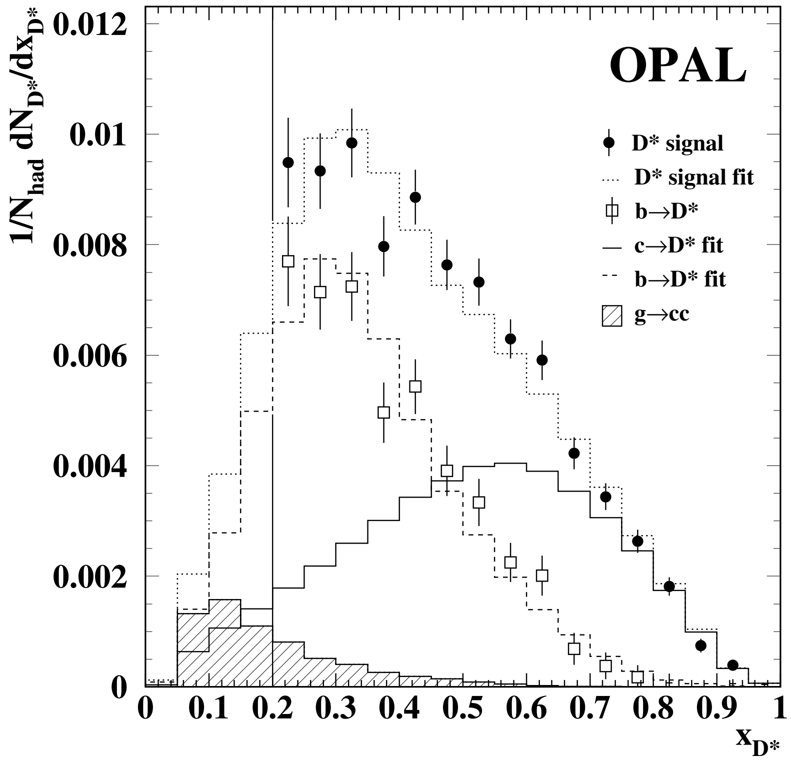

Figure 4: Efficiency corrected yield of D^{*+} mesons as a function of the scaled energy $x_{D^{*+}}$, $1/N_{had} dN_{D^{*+}}/dx_{D^{*+}}$, for all candidates (filled points with error bars) reconstructed in the decay $D^{*+} \to D^0\pi^+, D^0 \to K^-\pi^+$, and the charm component after flavour separation (solid line). The open points are the bottom component, and the dashed line represents the result of the fit. Also shown is the predicted contribution from gluon splitting events (hatched area). The reconstruction is only done for $x_{D^{*+}} > 0.2$, as indicated by the solid vertical line.

and correcting for the branching ratios $B(D^{*+} \to D^0\pi^+) = 0.683 \pm 0.014$ and $B(D^0 \to K^-\pi^+) = 0.0383 \pm 0.0012$ [22], the total multiplicity of D^{*+} mesons in hadronic Z^0 decays is found to be

$$\bar{n}_{Z^0 \to D^{*+}X} = 0.1854 \pm 0.0041 \ . \tag{11}$$

In addition the shape of the fragmentation function allows the determination of the average $x_{D^{*+}}$ between 0 and 1 in charm decays to be measured as

$$\langle x_{D^{*+}} \rangle_c = 0.515 \pm 0.002 \ . \tag{12}$$

Again only the statistical error is quoted. Note that this measurement does not include the effects from D^* mesons produced in gluon splitting.

5.3 Systematic Errors of the Measurement of D^{*+} Production

A number of systematic errors are investigated in connection with the D^{*+} rate measurements in charm and in bottom events. Note that the errors are totally anticorrelated, and only the ones for the rate in $Z^0 \to c\bar{c}$ events are given. Errors of the determination of the mean scaled energy of D^{*+} mesons are discussed separately at the end of this section. The first group of errors are due to detector effects, resolutions and Monte Carlo modelling:

- Track quality cuts: The effects of the track quality cuts are investigated by comparing the efficiency for each selection cut in data and Monte Carlo. An error of $\pm 0.6\%$ has been found to be sufficient to cover observed differences.

- Fraction of silicon hits: The resolution of secondary vertices depends on the fraction of tracks which use measurements from the silicon micro-vertex detector. The fraction in Monte Carlo events has been re-weighted to the one measured in data. An error of $\pm 0.4\%$ is derived from the statistical precision of this procedure.

- $\mathrm{d}E/\mathrm{d}x$ modelling: The calibration of the specific energy loss, $\mathrm{d}E/\mathrm{d}x$, has been compared in data and Monte Carlo in samples of identified particles. Samples of kaons and pions are selected in decays of $\phi \to K^-K^+$ and $K^0 \to \pi^+\pi^-$ mesons without using $\mathrm{d}E/\mathrm{d}x$ requirements, and the calibration of $\mathrm{d}E/\mathrm{d}x$ is measured in the data. In addition D^{*+} mesons are reconstructed without $\mathrm{d}E/\mathrm{d}x$ requirements, and the results are compared with those quoted in table 2. For the applied cut of 2% on the kaon weight an error of 1.1% of the total rate was found in those candidates where a cut was applied. This error contains a contribution from the measurement of $\mathrm{d}E/\mathrm{d}x$ itself, mainly due to the calibration, and from the requirement of at least 20 hits for the $\mathrm{d}E/\mathrm{d}x$ measurement. Since a $\mathrm{d}E/\mathrm{d}x$ cut is only used for $x_{D^{*+}} < 0.5$ this translates into a reduced error on the total rate in charm events of 0.8%, and in bottom events of 1.0%.

- Mass resolution: The invariant mass resolutions in data and Monte Carlo for the decay selected have been compared. The M_0 resolution in the Monte Carlo is 27.5 MeV, the one in data 27.9 MeV. Depending on the Monte Carlo sample used variations in the mass resolution from sample to sample of up to a few MeV are observed. These differences correspond to changes in the momentum resolution of the detector of approximately 10%, and translate into a systematic error on the efficiency of 1.0%.

- Rate of partially reconstructed D^{*+}: The total contribution from partially reconstructed D^{*+} mesons is measured in the fit to be $(8.1 \pm 1.7)\%$ in the selected sample. Of these $(4.6 \pm 0.8)\%$ are reconstructed as coming from the satellite decay mode. The Monte Carlo simulation predicts the fraction of partially reconstructed D^{*+} decays to be $(7.9 \pm 0.5)\%$, of which $(4.8 \pm 0.4)\%$ are from the satellite decay mode. The rest, $(3.3 \pm 0.3)\%$, are from a number of other decays, as discussed in section 5.1. In general very good agreement is observed between the predicted and the measured fractions, both within the Monte Carlo simulation, and between data and Monte Carlo. The uncertainty of the method is estimated from the statistical precision of the fit, and from the error of the individual branching ratios contributing to the partially reconstructed signal in the Monte Carlo. In addition a contribution of 0.5% is included to account for the finite Monte Carlo statistics available for this study. In total the relative error of the rate of partially reconstructed D^{*+} mesons contributing to the signal is estimated to be 22% of the rate of partially reconstructed mesons, which contributes an error of 1.5% to the total rate measurement.

- Background subtraction: The combinatorial background in the sample is subtracted based on estimators derived from data. The quality of the procedure has been studied in the

Monte Carlo simulation. Within the available statistics no significant deviations are found. The total difference is less than 1%, and an error of 1% is assigned to this source.

- $g \to c\bar{c}$: The expected contribution from gluon splitting has been subtracted from the sample, for $x_{D^{*+}} > 0.2$. The mean value used is the one measured in [7,24] of 0.0238 ± 0.0048. The contribution from this process has been varied within this error, which results in an error on the total rate of $\pm 1\%$. Monte Carlo studies indicate that the shape of the $g \to c\bar{c}$ component is not very dependent on the particular Monte Carlo model used. Comparing JETSET and the Ariadne Monte Carlo model [26] an error of $\pm 1\%$ is assigned to this source, resulting in a total error from gluon splitting of $\pm 1.4\%$.

- Heavy flavour fragmentation: The total rate of D^{*+} mesons produced in $Z^0 \to c\bar{c}$ and in $Z^0 \to b\bar{b}$ decays has been obtained by integrating the fitted fragmentation functions from $x_{D^{*+}} = 0$ to 1. This procedure is subject to a number of systematic uncertainties:

  - fragmentation function: The Peterson fragmentation function has been used for the results quoted. The different fragmentation models of Collins and Spiller [27] and Kartvelishvili [28] have been used to estimate its influence. The largest difference in the fitted rate has been used as the systematic error from this source. The error found is 1% of the rate in charm events, and 4% in bottom events.

    As a cross-check the fits have been repeated using the QCD inspired fragmentation function from Nason et al. [29]. The results are compatible with the ones obtained using the fragmentation models. The error on the fitted parameters however also reflect the limited statistics available for the initial tune of the model using low energy data. It is therefore used as a cross-check rather than to give an additional error.

  - b decay modelling: A comparatively large fraction of $b \to D^{*+}$ decays are not observed since only events with $x > 0.2$ are considered in this analysis. In addition to the error from different fragmentation models discussed above, an error introduced by this extrapolation on the measured b-rate has been studied as in [8] by considering the different types of decays contributing to the spectrum, and investigating the differences in the extrapolation introduced by each of the components. The differences found amount to an error of 2% on the $b \to D^*$ rate measurement.

  - excited D meson production: The shape of the fragmentation functions is influenced by the presence of D excited states in the decay chains. About 32% of all D^{*+} mesons have been measured as originating in decays of excited charm mesons. The contribution from these has been varied by $\pm 18\%$ around the mean value of 32%, as was done in [8]. The resulting error is 0.2% on the rate.

  The total error from all fragmentation modelling issues is 3% for charm, 5% for bottom.

In addition the errors discussed in the section on the flavour separation apply to the rate measurements as well. A complete breakdown of errors for the measurements is given in table 3.

Only a few of the errors listed for the rate measurement have a significant effect on the determination of the mean scaled energy of D^{*+} mesons in charm decays. The most important error comes from the extrapolation of the fragmentation function into the unmeasured region below $x_{D^{*+}} = 0.2$. Making the same comparisons between different fragmentation models as

	charm	bottom	$\overline{n}_{Z^0 \to D^{*+}}$	$\langle x_{D^{*+}} \rangle_c$
error source	$\times 10^{-3}$			
detector resolution				
track quality cuts	0.006	0.008	0.0008	
fraction of silicon hits	0.003	0.004	0.0004	0.001
$\mathrm{d}E/\mathrm{d}x$ modelling	0.008	0.013	0.0012	
total detector resolution	0.011	0.016	0.0015	0.001
D^{*+} *reconstruction*				
mass resolution	0.010	0.013	0.0013	
subtracting partially reconstructed decays	0.016	0.020	0.0019	0.002
D^{*+} background subtraction	0.010	0.013	0.0013	
$g \to c\bar{c}$	−0.016	−0.019	−0.0018	0.004
total D^{*+} reconstruction	0.026	0.030	0.0032	0.005
flavour separation				
f_b statistical error	0.010	0.013		
background modelling	0.017	0.023		
hemisphere correlation	0.004	0.005		
charm modelling	0.010	0.013		
bottom multiplicity	−0.005	+0.007		0.002
charm multiplicity	+0.006	−0.008		
bottom lifetime	−0.007	+0.009		
charm lifetime	+0.003	−0.004		
B mixing	0.003	0.004		
fragmentation model	0.012	0.053	0.0041	0.007
b decay model		0.027	0.0021	
excited D meson production	0.002	0.003	0.0003	0.002
total flavour separation	0.030	0.070	0.0047	0.008
total	0.040	0.078	0.0059	0.009

Table 3: List of systematic errors relevant in the determination of the rate of D^{*+} mesons produced in $Z^0 \to c\bar{c}$ and in $Z^0 \to b\bar{b}$ events, the total multiplicity of D^{*+} mesons in Z^0 decays, and the mean scaled energy. For the error of the mean scaled energy only errors which are larger than 0.001×10^{-3} are listed separately, otherwise the total contribution from a class of errors is given. A sign in front of an error indicates the direction of change under a positive change of the variable. The last three errors from the flavour separation include the contribution from the same sources through the D^{*+} reconstruction. Note that all flavour separation errors are anti-correlated between the charm and the bottom result.

described above a modelling error of ± 0.007 for the mean scaled energy has been determined. The uncertainty in the modelling of gluon splitting results in a further error of 0.004. Effects related to the flavour separation have much less of an effect on the mean scaled energy. Taken together all other errors except the above-mentioned modelling issues contribute another 0.004 to the error. The reconstruction of D^{*+} mesons, in particular the background subtraction, contribute an additional overall error of 0.002.

The final results, including all systematic errors, for the hadronisation fractions of charm and bottom quarks into D^{*+} mesons are found to be

$$\Gamma_{c\bar{c}}/\Gamma_{had} \cdot f\,(c \to D^{*+}X)\;B(D^{*+} \to D^0\pi^+)\;B(D^0 \to K^-\pi^+) = (1.041 \pm 0.020 \pm 0.040) \times 10^{-3} \ ,$$

and

$$\Gamma_{b\bar{b}}/\Gamma_{had} \cdot f\,(b \to D^{*+}X)\;B(D^{*+} \to D^0\pi^+)\;B(D^0 \to K^-\pi^+) = (1.334 \pm 0.049 \pm 0.078) \times 10^{-3} \ ,$$

where the first error is statistical, the second systematic. The total multiplicity of D^{*+} mesons in hadronic Z^0 decays is found to be

$$\bar{n}_{Z^0 \to D^{*+}X} = 0.1854 \pm 0.0041 \pm 0.0059 \pm 0.0069 \ .$$

The last error quoted is due to external branching ratios. From the shape of the fragmentation function the average mean scaled energy $x_{D^{*+}}$ of D^{*+} mesons in charm decays is determined to be

$$\langle x_{D^{*+}} \rangle_c = 0.515 \pm 0.002 \pm 0.009 \ .$$

The errors quoted are statistical and systematic, respectively. The results quoted is for the primary production of D^{*+} mesons in $Z^0 \to c\bar{c}$ events, and does not contain contributions from gluon splitting events. The results are in agreement with other measurements at LEP and with the previous OPAL determination [7,30,31].

6 Measurement of $f\,(c \to D^{*+}X)$, $f\,(b \to D^{*+}X)$ and of $\Gamma_{c\bar{c}}/\Gamma_{had}$

The hadronisation fraction $f\,(c \to D^{*+}X)$ is measured by the simultaneous detection of charm quarks in two jets of the event. In one jet, a charm meson candidate is identified by using the exclusive D^{*+} meson tag discussed in section 4.1. In the other jet the inclusive tag presented in section 4.2 is used. Background is suppressed by requiring that both D^{*+} tags are of opposite charge where the charge of the D^{*+} is given through the charge of the slow pion candidate from the $D^{*+} \to D^0\pi^+$ decay. By determining both the number of exclusively reconstructed D mesons and of simultaneously tagged jets, the hadronisation fraction can be calculated.

The hadronisation fraction $f\,(b \to D^{*+}X)$ is measured in an analogous fashion by the simultaneous detection of a lepton in one jet and an inclusively reconstructed D^{*+} meson in another jet of the event. The exclusive charm tag is replaced by a lepton tag, optimised for the selection of bottom events. The inclusive tag based on the slow pion is used in the opposite jet.

Combining the hadronisation fraction $f\,(c \to D^{*+}X)$ with the measurement of the production of D^{*+} mesons in $Z^0 \to c\bar{c}$ events the relative charm partial width $\Gamma_{c\bar{c}}/\Gamma_{had}$ is calculated, as discussed at the end of this section.

6.1 The Tagged Samples

Two samples are used in this analysis, one tagged by the presence of an exclusively reconstructed D^{*+} meson, the other tagged by a lepton. Both are selected as described in section 4. After all cuts a sample of 27 005 D^{*+} candidates has been found, of which $11\,366 \pm 107$ are estimated background events. Of the selected D^{*+} events a fraction of 0.774 ± 0.023 are reconstructed as coming from $Z^0 \rightarrow c\bar{c}$ events. The number of tagged electron and muon candidates is determined to be 43 579, of which 4445 ± 64 do not originate in bottom decays.

Slow pions are sought in the secondary jet in the samples of events tagged by either a D^{*+} meson or a lepton. The reconstruction of slow pion candidates proceeds as described in section 4.2. Event samples are prepared for the correct charge combination D^{*+}-π^- and for any charge combination ℓ-π, respectively. Background in the slow pion sample is estimated from a D^{*-}-π^- sample, prepared using a selection in a sideband of $\Delta M > 0.18$. A clear enhancement is visible at low values of p_t^2 as shown in figure 5(a) for the D^{*+} tag, and in figure 5(b) for the lepton tag. A much smaller enhancement is visible in the sideband selected double tag, shown in figure 5(c). The number of double tagged candidates, counted below $p_t^2 < 0.01$ GeV^2, is 2146 D^{*+}-π^+ candidates, and 5502 ℓ-π candidates.

The efficiency to reconstruct a slow pion in the presence of a fully reconstructed D^{*+} meson or a lepton in the other jet is determined in Monte Carlo simulated events. The slow pion is sought in the secondary jet of the event, and its reconstruction efficiency is calculated. This procedure is done individually in each of the five exclusive D^{*+} modes, and for the lepton tagged sample. The final efficiency is calculated by reweighting the Monte Carlo efficiencies to reflect the mixture of tagged events in the data. After all cuts the efficiencies are found to be

$$\epsilon^{c}_{D^*\pi} = 0.384 \pm 0.004 \quad \text{and} \quad \epsilon^{b}_{D^*\pi} = 0.189 \pm 0.006 \ , \tag{13}$$

for $c \rightarrow D^{*+}$ and $b \rightarrow D^{*+}$ events, respectively. In lepton tagged events the efficiencies are

$$\epsilon^{c}_{\ell\pi} = 0.414 \pm 0.029 \quad \text{and} \quad \epsilon^{b}_{\ell\pi} = 0.193 \pm 0.005 \ . \tag{14}$$

The errors quoted are purely statistical.

6.2 Composition of the Double Tagged Sample

A number of different classes of events contribute to the sample of double tagged events. At very low p_t^2 a significant fraction of the candidates are due to slow pions from the decay $D^{*+} \rightarrow D^0\pi^+$, both in charm and in bottom decays. The signal in bottom decays, while similar to the one in charm, has a broader distribution in p_t^2. Background in the sample comes from a number of different processes. The dominant source is random tracks that pass the applied cuts. This combinatorial background falls significantly more slowly with increasing p_t^2 than does the signal, and does not exhibit the characteristic enhancement at very low p_t^2.

A small but important background is slow pions from fake double tag candidates. A double tagged event is denoted a "fake double tag", if the slow pion candidate found in the inclusive tag is correctly identified, but the fully reconstructed D^{*+} meson or the lepton in the other jet is wrongly identified. Such events contribute to the peak in the p_t^2 spectrum, and need to be subtracted from the sample.

In the following each of the different parts of the candidate distribution will be briefly discussed. In the last part of this section the method used to count the number of double tags from charm decays is presented.

6.2.1 Combinatorial Background and Fake Estimation

The combinatorial background is the dominant background source. Its shape is estimated using events with the wrong charge correlation between the D^{*+} and the slow pion in the opposite hemisphere, which in addition are reconstructed in a sideband of ΔM on the exclusive side, between 0.18 (0.19) GeV $< \Delta M <$ 0.20 (0.22) GeV (numbers in brackets are for the semileptonic channels). Searching for slow pions in the secondary jet relative to the exclusive candidates tagged in the sidebands, a signal for charm production is observed at low p_t^2 (figure 5(c)). This signal has two contributions, one from fake double tags, another small one from incompletely reconstructed D^{*+} meson decays in the D-jet. In both cases a true slow pion is found in the secondary jet. The total fraction of fake double tags in the background is measured in the sidebands, and is subtracted from the total number of double tags, as described in 6.3.

6.2.2 Contribution from Bottom Events

The shape of the p_t^2 signal in bottom events is determined in data from the lepton-slow pion double tagged sample, which is about 90% pure in bottom decays. The fraction of events in the D^{*+}-π^- double tagged sample originating from bottom decays is determined from the known fraction of b-events in the D^{*+} sample, and the efficiency to tag a slow pion in a b-decay in the secondary jet.

The situation is slightly complicated by mixing in the neutral B system. If mixing has occurred in either hemisphere, the charge correlation between the primary quark and the corresponding D^{*+} mesons is changed, and the correlation between the charge of the slow pion track and the fully reconstructed D^{*+} candidate is opposite to the unmixed case. This fraction of events migrates out of the signal sample in this analysis. The total probability in bottom events that mixing has destroyed the charge correlation is given by

$$\chi_{\mathrm{eff}}^{\mathrm{D}^{*+}} = \chi_{\mathrm{D}^{*+}}(1 - \chi_{\pi^+_{\mathrm{slow}}}) + \chi_{\pi^+_{\mathrm{slow}}}(1 - \chi_{\mathrm{D}^{*+}}) \tag{15}$$

where $\chi_{\pi^+_{\mathrm{slow}}}, \chi_{\mathrm{D}^{*+}}$ are the effective mixing parameters applicable to the slow pion and the D^{*+} sample, respectively. The two mixing parameters are equal, since a D^{*+} tag is used in both jets. The majority of D^{*+} mesons in $Z^0 \rightarrow b\overline{b}$ events originate from decays of the B^0 meson. This fraction is estimated using semileptonic B decays to be $r_{\mathrm{d}} = 0.790^{+0.13}_{-0.12}$ [32]. A small percentage of D^{*+} mesons are also expected from B_s mesons, which also mix. The number of D^{*+} from B_s mesons was estimated to be $r_{\mathrm{s}} = 0.033 \pm 0.015$. The average mixing in the neutral B system is determined from the world average value for the mixing parameter, $\chi_{\mathrm{d}} = 0.175 \pm 0.016$ [22]. For the mixing parameter of the B_s meson the current world average limit of $\chi_{\mathrm{s}} > 0.49$ at 95% confidence level [22] has been used. In this analysis χ_{s} is varied between 0.49 and 0.50. The effective mixing seen by the D^{*+} mesons is given by

$$\chi_{\mathrm{D}^{*+}} = r_{\mathrm{d}}\, \chi_{\mathrm{d}} + r_{\mathrm{s}}\, \chi_{\mathrm{s}}. \tag{16}$$

In addition D^{*+} mesons with the wrong sign can be produced in bottom decays, when a $\overline{c}$ quark is produced in the decay of the W. This can be expressed in terms of a mixing-like parameter ζ_{D}. As in [7] a value of $\zeta_{\mathrm{D}} = 0.025 \pm 0.025$ is used. The effective mixing parameter for the D^{*+}-π^- double tag sample is estimated to be

$$\chi_{\mathrm{eff}}^{\mathrm{D}^{*+}} = 0.289 \pm 0.050. \tag{17}$$

This number is in agreement with a direct measurement of the effective D^{*+} mixing in [18].

6.3 Determination of the Number of Double Tags

The number of double tagged events in the sample is estimated from the three p_t^2 distributions by a simultaneous fit. The right sign sample is fitted as a superposition of true signal from charm and bottom decays, a contribution from fake double tagged events, and background. Each of the individual contributions is described by an exponential function

$$F(p_t^2)_{j=\mathrm{bgd,b,c}} = a_j \;\exp(b_j p_t^2) \; . \tag{18}$$

The parameters of the signal originating from bottom decays is determined in the ℓ-π double tagged sample. The fake distribution is measured in a double tagged sideband sample, where the exclusive candidates are selected in a sideband of ΔM. Combinatorial background is fitted for in the different distributions.

All three distributions are simultaneously fitted using the following parametrisations. The shape of the lepton tagged spectrum is parametrised by

$$F(p_t^2)_{\ell\pi} = F(p_t^2)_{\mathrm{bgd}} + f_{\mathrm{b}}^{\ell}\,\mathrm{f}\,(\mathrm{b} \to \mathrm{D}^{*+}\mathrm{X})\;F(p_t^2)_{\mathrm{b}}\;\epsilon_{\ell\pi}^{\mathrm{b}} + f_{\mathrm{c}}^{\ell}\,\mathrm{f}\,(\mathrm{c} \to \mathrm{D}^{*+}\mathrm{X})\;F(p_t^2)_{\mathrm{c}}\;\epsilon_{\ell\pi}^{\mathrm{c}} \; , \tag{19}$$

where the purities f_{c}^{ℓ} and f_{b}^{ℓ} have been given in section 4.3, and $\epsilon_{\ell\pi}^{\mathrm{b}}, \epsilon_{\ell\pi}^{\mathrm{c}}$ are the efficiencies to find a slow pion in the secondary jet in the presence of a lepton in the other jet, in $\mathrm{b\overline{b}}$ and $\mathrm{c\overline{c}}$ events respectively, as quoted in section 6.1. Since both relative signs between leptons and pions are used eq. 19 does not depend on the mixing in the lepton tagged sample. The right sign signal distribution is described by

$$\begin{aligned} F(p_t^2)_{\mathrm{D}^*\pi} = &\quad F(p_t^2)_{\mathrm{bgd}} + F(p_t^2)_{\mathrm{fake}} \\ &+\; (1-\chi_{\mathrm{eff}}^{\mathrm{D}^{*+}})\,(1-f_{\mathrm{c}}^{\mathrm{D}^{*+}})\,\mathrm{f}\,(\mathrm{b} \to \mathrm{D}^{*+}\mathrm{X})\;F(p_t^2)_{\mathrm{b}}\;\epsilon_{\mathrm{D}^*\pi}^{\mathrm{b}} \\ &+\; f_{\mathrm{c}}^{\mathrm{D}^{*+}}\;\mathrm{f}\,(\mathrm{c} \to \mathrm{D}^{*+}\mathrm{X})\;F(p_t^2)_{\mathrm{c}}\;\epsilon_{\mathrm{D}^*\pi}^{\mathrm{c}} \; . \end{aligned} \tag{20}$$

The charm fraction $f_{\mathrm{c}}^{\mathrm{D}^{*+}}$ fulfils the condition $f_{\mathrm{c}}^{\mathrm{D}^{*+}} = (1 - f_{\mathrm{b}}^{\mathrm{D}^{*+}})$, and $\epsilon_{\mathrm{D}^*,\pi}^{\mathrm{c}}$, $\epsilon_{\mathrm{D}^*,\pi}^{\mathrm{b}}$ are the efficiencies to find a slow pion in the presence of a D^{*+} meson in the other jet in $\mathrm{c\overline{c}}$ and $\mathrm{b\overline{b}}$ events respectively. The mixing probability $\chi_{\mathrm{eff}}^{\mathrm{D}^{*+}}$ has been determined in section 6.2.2.

The contribution from fake double tags in the $\mathrm{D}^{*+} - \pi^-$ double tagged sample is measured in the sideband tagged sample, as described above. The p_t^2 spectrum in the sideband tagged sample is parametrised by

$$F(p_t^2)_{\mathrm{side}} = \alpha \;(F(p_t^2)_{\mathrm{bgd}} + \; F(p_t^2)_{\mathrm{fake}}) \; , \tag{21}$$

where $F(p_t^2)_{\mathrm{fake}}$ contains contributions from fakes in the double tagged sample and from partially reconstructed D^{*+} mesons. The contribution from fake double tags is assumed to have the flavour composition as the real signal, as given by the two last lines of eq. 20, and the same functions are used for $F(p_t^2)_{\mathrm{fake}}$ as for signal events. The absolute contribution from the fakes is obtained by rescaling the fitted fake contribution by the ratio α of the number of background candidates in the sideband sample to that in the signal sample.

Equations 19, 20 and 21 are fitted simultaneously. Free parameters in the fit are the hadronisation fractions $\mathrm{f}\,(\mathrm{c} \to \mathrm{D}^{*+}\mathrm{X})$ and $\mathrm{f}\,(\mathrm{b} \to \mathrm{D}^{*+}\mathrm{X})$, the normalisation of the fake rate, the shape parameters a and b of bottom and charm slow pion signals, and the background parameters. The different spectra are illustrated in figures 5(a) to (c), with the results of the fit superimposed in each case. The number of double tagged events in the D^{*+}-π^- double tagged sample in $\mathrm{Z}^0 \to \mathrm{c\overline{c}}$ events, $N_{\mathrm{D}^{*+},\pi^-}^{\mathrm{c}}$, and in the ℓ-π tagged sample, $N_{\ell,\pi}^{\mathrm{b}}$, are determined by

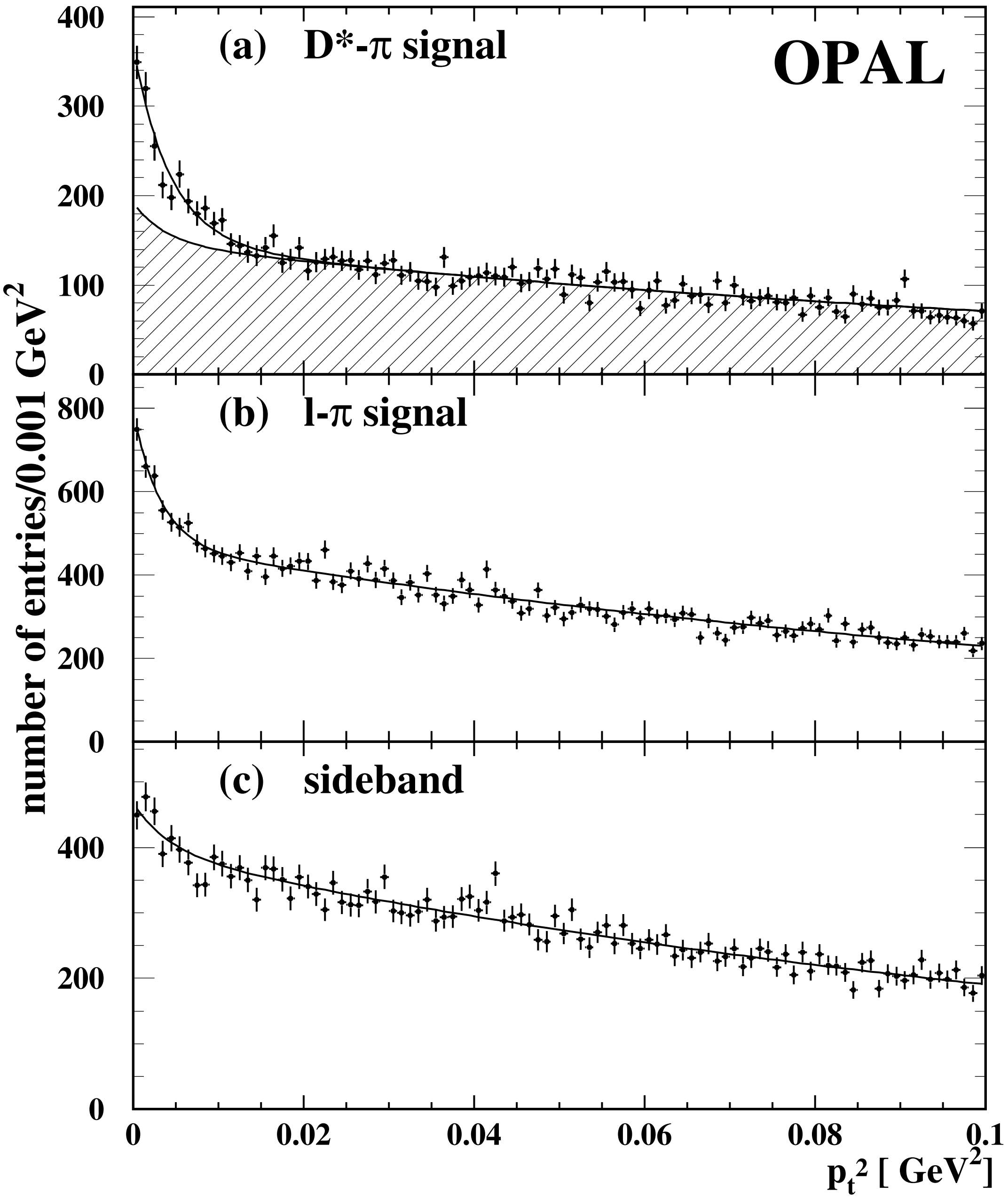

Figure 5: Spectrum of the squared transverse momentum of double tagged candidates after applying all cuts of the (a) signal candidates, reconstructed with opposite charges in both jets. The non-charm component is indicated by the hatched area; (b) lepton-tagged candidates. The points are the data and the lines the results of the fit; (c) background candidates, reconstructed in ΔM sidebands.

integrating the fitted signal functions in the double tagged samples between $p_t^2 = 0$ GeV^2 and $p_t^2 = 0.01$ GeV^2. They are found to be $N^{\mathrm{c}}_{\mathrm{D}^*\pi} = 702 \pm 44$, over a background of 1444 ± 18 events, and $N^{\mathrm{b}}_{\ell\pi} = 934 \pm 80$ over a background of 4568 ± 45 events, respectively. Correcting for the branching ratio $\mathrm{B}(\mathrm{D}^{*+} \to \mathrm{D}^0\pi^+) = 0.683 \pm 0.014$ [22] the hadronisation fractions are found to be

$$\begin{aligned} \mathrm{f}\,(\mathrm{c} \to \mathrm{D}^{*+}\mathrm{X}) &= 0.222 \pm 0.014 \\ \mathrm{f}\,(\mathrm{b} \to \mathrm{D}^{*+}\mathrm{X}) &= 0.173 \pm 0.016 \ , \end{aligned}$$

where the error quoted is only statistical.

Combining the measurement of the hadronisation fraction $\mathrm{f}\,(\mathrm{c} \to \mathrm{D}^{*+}\mathrm{X})$ with the result for the total rate of D^{*+} mesons in $\mathrm{Z}^0 \to \mathrm{c\bar{c}}$ events the charm partial width relative to the total hadronic width of the Z^0 is found to be

$$\Gamma_{\mathrm{c\bar{c}}}/\Gamma_{\mathrm{had}} = 0.180 \pm 0.011 \ ,$$

where the error quoted is purely statistical.

6.4 Systematic Errors

In this section the different sources of systematic errors for this part of the analysis are discussed. A full breakdown of all errors considered is given in table 4.

- Detector resolution effects: The effects of detector resolution modelling have been discussed in section 4.1.5. The total error applicable from these sources to this measurement is $\pm 1.8\%$, with the $\mathrm{d}E/\mathrm{d}x$ error being dominant.

- Flavour separation: The systematic errors of the flavour separation determined in section 4.1.5 are used to determine the corresponding systematic errors on the hadronisation fractions. Many of the errors for $\Gamma_{\mathrm{c\bar{c}}}/\Gamma_{\mathrm{had}}$ are correlated to that of the charm hadronisation fraction. This correlation is taken into account in calculating the final errors.

- Lepton identification: The systematic errors discussed in connection with the lepton identification are applicable to the measurement of $\mathrm{f}\,(\mathrm{b} \to \mathrm{D}^{*+}\mathrm{X})$.

- D^{*+} reconstruction: $\Gamma_{\mathrm{c\bar{c}}}/\Gamma_{\mathrm{had}}$ depends on the total rate of D^{*+} in Z^0 events. All errors discussed in section 5 are applicable to this measurement as well.

A number of additional errors are introduced through the inclusive charm tag:

- Heavy flavour fragmentation: The efficiency for finding slow pions in $\mathrm{Z}^0 \to \mathrm{c\bar{c}}$ events has been calculated in Monte Carlo. Systematic errors from the modelling of the heavy flavour fragmentation are studied as described in section 5.3. The total error from this source is $\pm 1.4\%$ on the slow pion efficiency. In table 4 this error is combined with the fragmentation error from the b/c separation.

- Excited D meson modelling: The influence of excited D meson production on the slow pion efficiency is studied as described in section 5.3, resulting in an efficiency error of 0.1%.

Source	$f(b \to D^{*+}X)$	$f(c \to D^{*+}X)$	$\Gamma_{c\bar{c}}/\Gamma_{had}$
detector resolution			
track quality cuts	0.0000	0.0000	0.0011
dE/dx modelling	0.0017	0.0025	0.0018
detector resolution	0.0010	0.0013	0.0009
flavour separation			
f_b stat error	0.0002	0.0022	0.0025
background modelling	0.0003	0.0030	0.0028
hemisphere correlation	< 0.0001	0.0007	0.0007
charm modelling	0.0002	0.0018	0.0017
bottom multiplicity	< 0.0001	-0.0009	-0.0008
charm multiplicity	0.0001	$+0.0011$	$+0.0010$
bottom lifetime	0.0001	-0.0012	-0.0011
charm lifetime	0.0002	$+0.0011$	$+0.0008$
fragmentation modelling	< 0.0001	0.0011	0.0018
lepton reconstruction			
lepton fragmentation	0.0030	< 0.0001	
bottom fraction in Z^0 decays	0.0017	< 0.0001	
lepton decay model	0.0050	< 0.0001	
semi-leptonic BR	0.0010	< 0.0001	
lepton fake rate	0.0020	< 0.0001	
D^{*+} *reconstruction*			
mass resolution			0.0018
subtracting partially reconstructed decays			0.0027
D^{*+} background subtraction			0.0018
double tag, slow pion reconstruction			
slow pion efficiency	0.0040	0.0010	0.0025
excited D meson production	0.0040	0.0010	0.0008
fitting procedure	0.0081	0.0104	0.0085
$B^0\overline{B^0}$ mixing	0.0002	0.0016	0.0011
jet resolution	0.0024	0.0031	0.0025
jet-jet correlation	0.0012	0.0015	0.0012
$g \to c\bar{c}$	< 0.0001	-0.0003	-0.0024
total error	0.0121	0.0133	0.0123
external inputs			
$B(D^{*+} \to D^0\pi^+)$	0.0034	0.0044	
$B(D^0 \to K^-\pi^+)$			0.0063

Table 4: List of systematic errors contributing to $f(c \to D^{*+}X)$, $f(b \to D^{*+}X)$ and $\Gamma_{c\bar{c}}/\Gamma_{had}$. A sign in front of an error indicates the direction of change under a positive change of the variable. A detailed explanation of the different errors can be found in the text.

- Jet definition: The resolution of the p_t^2 signal is dominated by the resolution of the direction of the jet axis. Possible modelling problems in the Monte Carlo have been checked by comparing the number of charged tracks and of neutral clusters used in the calculation of the jet axis. The Monte Carlo distributions have been re-weighted to the data distributions, and the efficiencies are re-determined. An error of 0.9% in charm, and 3% in bottom events has been found. As a cross-check the fit has been repeated fixing the fitted resolution[5] of the p_t^2 distribution of 0.056 GeV to its Monte Carlo value of 0.061 GeV. Consistent results have been found within the quoted errors.

- Jet-jet correlation: The efficiency for identifying a slow pion is influenced by the presence of an exclusively reconstructed D^{*+} meson in the other hemisphere. This bias is taken into account by calculating the efficiency in Monte Carlo in events where a D^{*+} meson has been reconstructed in the other hemisphere. A small error remains if the energy distribution of the secondary jet is not modelled properly in the Monte Carlo. This has been evaluated by reweighting the Monte Carlo energy distribution to that observed in the data, and recalculating the efficiency. The resulting error is 0.7% of the efficiency.

- Background subtraction and fitting procedure: Systematic effects introduced by the fitting procedure for background determination in the double tagged sample have been studied in Monte Carlo simulation.

  - The complete fit has been repeated in Monte Carlo. The number of double tags reconstructed is well reproduced within its statistical errors. The difference is 0.5%, and this is used an additional systematic error.
  - The modelling of the combinatorial background in the fit has been tested in the Monte Carlo by repeating the fit with the true Monte Carlo background. The fit has been done by either constraining the shape of the background to be the same in all double tagged samples, or by fitting it individually in each one. The observed difference of 2.5% has been assigned to this source.
  - The shape of the bottom component is estimated from the lepton sample. Possible biases have been investigated in the Monte Carlo by repeating the fit with the true bottom signal. The results agree to within 2%, and this has been used as the error.
  - The number of fake double tags predicted by the fit in the Monte Carlo has been compared to the known number of fake double tags. They agree to 10%. The number of fake double tags in the data has been measured in the fit to be $(8.5 \pm 2.2)\%$ of the combinatorial background. Monte Carlo predicts this to be $(9.9 \pm 0.8)\%$, which is compatible within errors with the measured rate. The error from this source is estimated by varying the fitted fake rate within its error, and by additionally assigning the difference between data and Monte Carlo as an systematic error. In total this gives an error of 3.5% of the signal in charm events, 3.0% in bottom events.
  - B-mixing: The uncertainty due to mixing in the neutral B sector has been studied by varying the effective mixing parameter χ_{eff} within its error, or 0.5% of the final result.
  - Fit function: As a cross check the analysis has been repeated with different parametrisations for both the signal and the background distributions. The background

[5] The resolution is defined as the width of the p_t^2 distribution at 50% of its maximum value.

is modelled using a polynomial $(a + b\ p_t^2 + c\ p_t^4)^{-1}$, and no differences are found for the results. The signal function has been replaced by a gaussian-like function $\exp(-(a + b\, p_t^2)^2)$, which also results in consistent results.

- $\mathrm{g} \rightarrow \mathrm{c\bar{c}}$: The contribution to the tagged samples from gluon splitting events has been discussed in section 5.3. It has been re-evaluated for the inclusively tagged jet, where Monte Carlo simulation predicts this to be $(0.64 \pm 0.08)\%$. A systematic error of 0.12% has been assigned to this source.

A list of all systematic errors is given in table 4.

7 Results and Conclusions

A double tagging technique has been used to measure the hadronisation fractions of charm and bottom quarks into charged $\mathrm{D}^{*\pm}$ mesons. They are determined to be

$$\begin{aligned} \mathrm{f}\,(\mathrm{c} \rightarrow \mathrm{D}^{*+}\mathrm{X}) &= 0.222 \pm 0.014 \pm 0.014 \pm 0.004\ , \\ \mathrm{f}\,(\mathrm{b} \rightarrow \mathrm{D}^{*+}\mathrm{X}) &= 0.173 \pm 0.016 \pm 0.012 \pm 0.003\ , \end{aligned}$$

where the first error quoted is statistical, the second systematic, and the third one due to external branching ratios.

From the number of $\mathrm{D}^{*\pm}$ mesons observed in the decay $\mathrm{D}^{*+} \rightarrow \mathrm{D}^0\pi^+, \mathrm{D}^0 \rightarrow \mathrm{K}^-\pi^+$ the multiplicity of D^{*+} mesons in hadronic Z decays is measured to be

$$\bar{n}_{\mathrm{Z}^0 \rightarrow \mathrm{D}^{*+}X} = 0.1854 \pm 0.0041 \pm 0.0059 \pm 0.0069\ .$$

Applying bottom tags based on lifetime, jet shape and hemisphere charge information in the event the charm and the bottom components have been separated, and the individual production rates are found to be

$$\begin{aligned} \Gamma_{\mathrm{c\bar{c}}}/\Gamma_{\mathrm{had}}\ \mathrm{f}\,(\mathrm{c} \rightarrow \mathrm{D}^{*+}\mathrm{X})\ \mathrm{B}(\mathrm{D}^{*+} \rightarrow \mathrm{K}^-\pi^+\pi^+) &= (1.041 \pm 0.020 \pm 0.040) \times 10^{-3}\ , \\ \Gamma_{\mathrm{b\bar{b}}}/\Gamma_{\mathrm{had}}\ \mathrm{f}\,(\mathrm{b} \rightarrow \mathrm{D}^{*+}\mathrm{X})\ \mathrm{B}(\mathrm{D}^{*+} \rightarrow \mathrm{K}^-\pi^+\pi^+) &= (1.334 \pm 0.049 \pm 0.078) \times 10^{-3}\ , \end{aligned}$$

The mean scaled energy of D^{*+} mesons in charm events is determined from the fragmentation function to be

$$\langle x_{\mathrm{D}^{*+}} \rangle_{\mathrm{c}} = 0.515 \pm 0.002 \pm 0.009\ .$$

From the hadronisation fraction $\mathrm{f}\,(\mathrm{c} \rightarrow \mathrm{D}^{*+}\mathrm{X})$ and the total production rate of D^{*+} mesons in $\mathrm{Z}^0 \rightarrow \mathrm{c\bar{c}}$ events, $\Gamma_{\mathrm{c\bar{c}}}/\Gamma_{\mathrm{had}}$ is found to be

$$\Gamma_{\mathrm{c\bar{c}}}/\Gamma_{\mathrm{had}} = 0.180 \pm 0.011 \pm 0.012 \pm 0.006\ .$$

Here the first error is statistical, the second one describes internal systematics, and the last one is due to branching ratio $\mathrm{B}(\mathrm{D}^0 \rightarrow \mathrm{K}^-\pi^+) = 0.0383 \pm 0.0012$ [22]. The correlations between the rate measurement and the hadronisation fraction are taken into account in this calculation. A detailed breakdown of the systematic error is given in table 4. The measurements presented in this paper are based on the full data sample of almost 4.4 million events collected with the OPAL detector at LEP at a centre-of-mass energy of about 91 GeV. For the first time the charm partial width has been measured without significant input from lower energy experiments, and in particular without assumptions about the centre-of-mass energy dependence of heavy flavour fragmentation. In a previous OPAL publication the hadronisation fraction $f(c \to D^{*+}X)$ was derived from measurements at lower energy e^+e^- machines to be $f(c \to D^{*+}X)_{\text{low energy}} = 0.262 \pm 0.019 \pm 0.010$, where the last error is from the branching ratios $B(D^{*+} \to D^0\pi^+)$ and $B(D^0 \to K^-\pi^+)$. Assuming that the only correlation between the low energy result and the result presented in this paper is from the branching ratio $B(D^* \to D^0\pi^+)$, the low energy number is 1.4 standard deviations higher than the OPAL one, which is compatible with the assumption that the sources of D^{*+} mesons at lower energies and at LEP energies are the same. If the low energy hadronisation fraction were to be used instead of the one measured by OPAL $\Gamma_{c\bar{c}}/\Gamma_{\text{had}}$ would be lower by 15%.

In conclusion good agreement is found with the prediction of the Standard Model [22] of $\Gamma_{c\bar{c}}/\Gamma_{\text{had}} = 0.172$, and with other measurements of the same quantities at LEP [6–8].

Acknowledgements

We particularly wish to thank the SL Division for the efficient operation of the LEP accelerator at all energies and for their continuing close cooperation with our experimental group. We thank our colleagues from CEA, DAPNIA/SPP, CE-Saclay for their efforts over the years on the time-of-flight and trigger systems which we continue to use. In addition to the support staff at our own institutions we are pleased to acknowledge the
Department of Energy, USA,
National Science Foundation, USA,
Particle Physics and Astronomy Research Council, UK,
Natural Sciences and Engineering Research Council, Canada,
Israel Science Foundation, administered by the Israel Academy of Science and Humanities,
Minerva Gesellschaft,
Benoziyo Center for High Energy Physics,
Japanese Ministry of Education, Science and Culture (the Monbusho) and a grant under the Monbusho International Science Research Program,
German Israeli Bi-national Science Foundation (GIF),
Bundesministerium für Bildung, Wissenschaft, Forschung und Technologie, Germany,
National Research Council of Canada,
Hungarian Foundation for Scientific Research, OTKA T-016660, T023793 and OTKA F-023259.

References

[1] ALEPH Collaboration, R. Barate et al., *A measurement of R_b using a lifetime-mass tag*, CERN PPE/97-017, submitted to Phys. Lett. **B**;
ALEPH Collaboration, R. Barate et al., *A measurement of R_b using five mutually exclusive tags*, CERN PPE/97-018, submitted to Phys. Lett. **B**.

[2] DELPHI Collaboration, P. Abreu et al., Z. Phys. **C70** (1996) 531.

[3] L3 Collaboration, O. Adriani et al., Phys. Lett. **B307** (1993) 237.

[4] OPAL Collaboration, K. Ackerstaff et al., Z. Phys. **C74** (1997) 1.

[5] ALEPH Collaboration, D. Busculic et al., Z. Phys. **C62** (1994) 179.

[6] DELPHI Collaboration, P. Abreu et al., Phys. Lett. **B252** (1990) 140;
DELPHI Collaboration, P. Abreu et al., Phys. Lett. **B295** (1992) 383.

[7] OPAL Collaboration, R. Akers et al., Z. Phys. **C67** (1995) 27.

[8] OPAL Collaboration, G. Alexander et al., Z. Phys. **C72** (1996) 1.

[9] OPAL Collaboration, K. Ackerstaff et al., *Measurement of the Branching Fractions and Forward-Backward Asymmetries of the* Z^0 *into Light Quarks* , CERN PPE/97-63, submitted to Z. Phys. **C**.

[10] OPAL Collaboration, K. Ahmet et al., Nucl. Instr. Meth. **A305** (1991) 275;
P.P. Allport et al., Nucl. Instr. Meth. **A324** (1993) 34;
P.P.Allport et al., Nucl. Instr. Meth. **A346** (1994) 476;
O. Biebel et al., Nucl. Instr. Meth. **A323** (1992) 169;
M. Hauschild et al., Nucl. Instr. Meth. **A314** (1992) 74.

[11] OPAL Collaboration, R. Akers et al., Z. Phys. **C65** (1995) 17.

[12] OPAL Collaboration, R. Akers et al., Z. Phys. **C63** (1994) 197.

[13] T. Sjöstrand, Comp. Phys. Comm. **82** (1994) 74.

[14] OPAL Collaboration, G. Alexander et al., Z. Phys. **C69** (1996) 543.

[15] C. Peterson et al., Phys. Rev. **D27** (1983) 105.

[16] The LEP Collaborations, ALEPH, DELPHI, L3 and OPAL, and the LEP Electroweak working group, Nucl. Instr. Meth., **A378** (1996) 101;
The LEP Collaborations, ALEPH, DELPHI, L3 and OPAL, and the LEP Electroweak Working Group, CERN-PPE/96-183, and references therein. This paper has been prepared by the LEP collaboration for presentation at major conferences, and contains some preliminary numbers.

[17] J. Allison et al., Nucl. Instr. Meth. **A317** (1991) 47.

[18] OPAL Collaboration, G. Alexander et al., Z. Phys. **C73** (1997) 379.

[19] OPAL Collaboration, G. Alexander et al., Z. Phys. **C70** (1996) 357.

[20] OPAL Collaboration, G. Alexander et al., Z. Phys. **C70** (1996) 357.

[21] OPAL Collaboration, R. Akers et al., Z. Phys. **C60** (1993) 199.

[22] Particle Data Group, Phys. Rev. **D54** (1996) 1.

[23] OPAL Collaboration, R. Akers et al., Z. Phys. **C65** (1995) 17.

[24] OPAL Collaboration, R. Akers et al., Phys. Lett. **B353** (1995) 595.

[25] DELPHI Collaboration, P. Abreu et al., Z. Phys. **C71** (1996) 539.

[26] L. Lönnblad, Comp. Phys. Comm. **71** (1992) 15.

[27] P.Collins, T.Spiller, J. Phys. **G11** (1985) 1289.

[28] V.G. Kartvelishvili, A.K. Likehoded, V.A. Petrov, Phys. Lett. **B78** (1978) 615.

[29] B. Mele, P. Nason, Phys. Lett. **B245** (1990) 635; Nucl. Phys. **B361** (1991) 626.

[30] ALEPH Collaboration, D. Buskulic et al., Phys. Lett. **B266** (1991) 218.

[31] DELPHI Collaboration, P. Abreu et al., Z. Phys. **C59** (1993) 533.

[32] OPAL Collaboration, P.D. Acton et al., Z. Phys. **C67** (1995) 379.